HAL
open science

Degassing vs. eruptive styles at Mt. Etna volcano (Sicily, Italy). Part I: Volatile stocking, gas fluxing, and the shift from low-energy to highly explosive basaltic eruptions

Roberto Moretti, Nicole Di Métrich, Ilenia Arienzo, Valeria Di Renzo, Alessandro Aiuppa, Patrick Allard

To cite this version:

Roberto Moretti, Nicole Di Métrich, Ilenia Arienzo, Valeria Di Renzo, Alessandro Aiuppa, et al.. Degassing vs. eruptive styles at Mt. Etna volcano (Sicily, Italy). Part I: Volatile stocking, gas fluxing, and the shift from low-energy to highly explosive basaltic eruptions. Chemical Geology, 2018, 482, pp.1-17. 10.1016/j.chemgeo.2017.09.017 . insu-01867376

HAL Id: insu-01867376

https://insu.hal.science/insu-01867376

Submitted on 4 Sep 2018

HAL is a multi-disciplinary open access archive for the deposit and dissemination of scientific research documents, whether they are published or not. The documents may come from teaching and research institutions in France or abroad, or from public or private research centers.

L'archive ouverte pluridisciplinaire **HAL**, est destinée au dépôt et à la diffusion de documents scientifiques de niveau recherche, publiés ou non, émanant des établissements d'enseignement et de recherche français ou étrangers, des laboratoires publics ou privés.

Accepted Manuscript

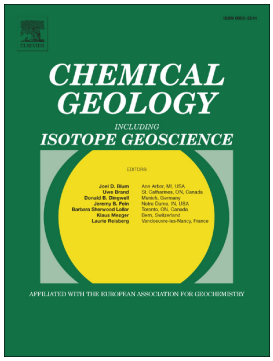

Degassing vs. eruptive styles at Mt. Etna volcano (Sicily, Italy). Part I: Volatile stocking, gas fluxing, and the shift from low-energy to highly explosive basaltic eruptions

Roberto Moretti, Nicole Métrich, Ilenia Arienzo, Valeria Di Renzo, Alessandro Aiuppa, Patrick Allard

PII: S0009-2541(17)30518-1
DOI: doi: 10.1016/j.chemgeo.2017.09.017
Reference: CHEMGE 18472

To appear in: *Chemical Geology*

Received date: 28 March 2017
Revised date: 4 September 2017
Accepted date: 12 September 2017

Please cite this article as: Roberto Moretti, Nicole Métrich, Ilenia Arienzo, Valeria Di Renzo, Alessandro Aiuppa, Patrick Allard , Degassing vs. eruptive styles at Mt. Etna volcano (Sicily, Italy). Part I: Volatile stocking, gas fluxing, and the shift from low-energy to highly explosive basaltic eruptions, *Chemical Geology* (2017), doi: 10.1016/j.chemgeo.2017.09.017

This is a PDF file of an unedited manuscript that has been accepted for publication. As a service to our customers we are providing this early version of the manuscript. The manuscript will undergo copyediting, typesetting, and review of the resulting proof before it is published in its final form. Please note that during the production process errors may be discovered which could affect the content, and all legal disclaimers that apply to the journal pertain.

ACCEPTED MANUSCRIPT

Degassing vs. eruptive styles at Mt. Etna volcano (Sicily, Italy). Part I: Volatile stocking, gas fluxing, and the shift from low-energy to highly explosive basaltic eruptions

Roberto Moretti[1], Nicole Métrich[2], Ilenia Arienzo[3], Valeria Di Renzo[1], Alessandro Aiuppa[4,5], Patrick Allard[2]

[1] *Dipartimento di Ingegneria Civile, Design, Edilizia e Ambiente, Università degli Studi della Campania "Luigi Vanvitelli", Via Roma 29, 81031 Aversa (CE), Italy*

[2] *Institut de Physique du Globe, Sorbonne-Paris Cité, Univ. Paris Diderot, UMR 7154 CNRS, 75005 Paris France.*

[3] *Istituto Nazionale di Geofisica e Vulcanologia, sezione Osservatorio Vesuviano, via Diocleziano 328, 80124 Napoli, Italy*

[4] *Dipartimento di Scienze della Terra e del Mare, Università di Palermo, Via Archirafi 36, 93100, Palermo, Italy*

[5] *Istituto Nazionale di Geofisica e Vulcanologia, sezione di Palermo, via U. La Malfa 32, 93100, Palermo, Italy*

Running title: Composite volatile patterns behind the eruptive style of Mt. Etna

Abstract

Basaltic magmas can transport and release large amounts of volatiles into the atmosphere, especially in subduction zones, where slab-derived fluids enrich the mantle wedge. Depending on magma volatile content, basaltic volcanoes thus display a wide spectrum of eruptive styles, from common Strombolian-type activity to Plinian events. Mt. Etna, in Sicily, is a typical basaltic volcano where the volatile control on such a variable activity can be investigated. Based on a melt inclusion study in products from Strombolian or lava-fountain activity to Plinian eruptions, here we show that for the same initial volatile content, different eruptive styles reflect variable degassing paths throughout the composite Etnean plumbing system. The combined influence of i) crystallization, ii) deep degassing and iii) CO_2 gas fluxing can explain the evolution of H_2O, CO_2, S and Cl in products from such a spectrum of activity. Deep crystallization produces the CO_2-rich gas fluxing the upward magma portions, which will become buoyant and easily mobilized in small gas-

ACCEPTED MANUSCRIPT

rich batches stored within the plumbing system. When reaching gas-dominated conditions (i.e., a gas/melt mass ratio of ~ 0.3 and $CO_{2,gas}/H_2O_{gas}$ molar ratio ~ 5), magma batches will erupt effusively or mildly explosively. In case of the 122 BC Plinian eruption, open-system degassing conditions took place within the plumbing system, such that earlier CO_2-fluxing determined gas accumulation on top of the magmatic system, likely followed by H_2O-fluxing further hydrating the shallow magma. The emission of such a cap in the early eruptive phase triggered the arrival of deep H_2O-rich magma whose fast decompression and bubble nucleation led to the highly explosive character, enhanced by abundant microlite crystallization and consequent increase of magma effective viscosity. This could explain why open system basaltic systems like Etna may experience highly explosive or even Plinian episodes during eruptions that start with effusive to mildly explosive phases. The proposed mechanism also determines a depression of chlorine contents in CO_2-fluxed (and less explosive) magmas with respect to those feeding Plinian events like 122 BC. The opposite is seen for sulfur: low to mild-explosive fluxed magmas are S-enriched, whereas the 122 BC Plinian products are relatively S-poor, likely because of early sulfide separation accompanying magma crystallization. The proposed mechanism involving CO_2 separation and fluxing may suggest a subordinate role for variable mixing of different sources having different degrees of K-enrichment. However, such a mechanism requires further experimental studies about the effects on S and Cl dissolution and does not exclude self-mixing between degassed and undegassed parcels within the Etna plumbing system. Finally, our findings may represent a new interpretative tool for the geochemical and petrologic monitoring of plume gas discharges and melt inclusions, and allow tracking the switch from mild-explosive to highly explosive or even Plinian events at Etna.

Keywords: Basaltic explosive volcanism, Mt. Etna, chemical thermodynamics, melt inclusions, total volatiles

ACCEPTED MANUSCRIPT

ACCEPTED MANUSCRIPT

1. Introduction

Explosive volcanism is generally related to a large amount of volatiles, i.e., a high gas/melt mass ratio in magmatic system, which strongly determines the regime under which the magma ascends to surface in open conduits (e.g., Houghton and Gonnermann, 2008). Most commonly, explosive basaltic volcanism occurs in arc environments, where the mantle source is enriched in fluids derived from subducted slabs (Métrich and Wallace, 2008). Improved understanding of how volatiles are released from a basaltic volcano experiencing a range of eruptive styles can provide key insights into physico-chemical changes occurring in the plumbing system when activity evolves from effusive, or mild-explosive, to high-explosive, or even Plinian, eruptions. For this purpose, a scan of volatile contents dissolved in melt inclusions (MIs) is mandatory to provide a petrological imaging of plumbing systems (e.g., Marianelli et al., 1999; Métrich et al., 2004; Spilliaert et al., 2006a; Mangiacapra et al., 2008; Moretti et al., 2013b), and to quantify total volatiles and their variations due to fluid transfer (essentially CO_2) throughout the system (e.g., Barsanti et al., 2009).

Mt. Etna basaltic volcano, located in Sicily (southern Italy), shows such a wide eruptive spectrum, related to the emission of volatile-rich alkali-basalts to hawaiitic magmas. In this work, we studied melt inclusions (MIs) hosted in olivine crystals from products extruded during: i) Bocca Nuova (BN) Strombolian activity in 1997-98, ii) the paroxysmal event of February 1999 from the South-East crater (SEC) (La Delfa et al, 2001), and iii) the 122 BC Plinian eruption (Coltelli et al. 1998; 2000). They have been analyzed in terms of major constituents, sulfur and chlorine concentrations and, for a subset of them, dissolved H_2O and CO_2 contents and sulfur speciation. The relationships with the sulfur redox state are treated in a companion paper (Moretti et al., submitted). The analysis of total (exsolved + dissolved) volatiles (H_2O^{TOT} and particularly CO_2^{TOT}) allows us to infer gas/melt variations in the system and characterize volatile abundances of the deep primitive magma source. This allows obtaining precious information on the evolution of degassing patterns of other volatiles components, such as S and Cl. Because such an evolution is greatly controlled by processes of CO_2 addition or loss, already occurring in the deep source, the results are used to

ACCEPTED MANUSCRIPT

discriminate –and switch among- the different degassing behaviors characterizing mildly and highly explosive, up to Plinian, events. The proposed analysis and modeling, here developed for conditions relevant to Mt. Etna, can be extended to other basaltic explosive volcanoes worldwide.

2. Geological background

2.1 Volcanological and geochemical outline

Mt. Etna, located at the boundary of the colliding African and European plates, is the largest and most active volcano of Europe. Its buildup is related to the rollback of the slab subducting under the Aeolian Islands (Doglioni et al. 1996). In the general classification of Mediterranean volcanism, Mt. Etna is considered as an example of anorogenic magmatism with hot-spot affinity (Peccerillo 2005). Mt. Etna alkali basalts to hawaiites are characterized by high contents of dissolved volatiles (Métrich et al. 2004; Spilliaert et al. 2006a, 2006b), as well as huge degassing rates at the surface, both as diffuse soil degassing from the volcano flanks and gas emissions from the summit crater plumes and fumarolic vents (Allard et al. 1991; Aiuppa et al. 2006; Giammanco et al. 1998). Mt. Etna volcanic gases show compositions unusually enriched in carbon and sulfur (and poor in water) relative to volcanoes in convergent settings, and have compositions intermediate between arc and hot-spot and divergent-plate volcanoes (Symonds et al. 1994). This peculiar gas signature suggests that the emitted alkaline magmas originate from a C-S-rich source, either of deep (e.g., a metasomatized mantle, likely related to the de-volatilization of the Ionian subducting slab; Tonarini et al. 2001) or shallow (crustal) provenance (see for instance Chiodini et al. 2011).

The volcanic history in the Etnean area probably began at about 500 ka, when both submarine and subaerial tholeiitic lavas were erupted in the so-called «Pre-etnean Gulf» (Condomines et al. 1982; Gillot et al. 1994). Since then, the erupted lavas gradually changed composition from subalkaline towards Na-alkaline. Mt. Etna's historic and recent (up to 1970) activity principally consisted of continuous degassing from the summit craters Bocca Nuova (BN), North-East Crater (NEC), South-

ACCEPTED MANUSCRIPT

East Crater (SEC), and Voragine (VOR) and frequent lava effusions and Strombolian eruptions of relatively low energy, both from the summit craters and from lateral vents that are chiefly concentrated in three rift zones (Kieffer 1985; Kieffer and Tanguy 1993; Tanguy and Kieffer 1993). Starting from the early 1970s, Mt. Etna has shown an escalation in eruptive frequency and magnitude (Allard et al. 2006a), associated with an increasingly alkaline and radiogenic signature of erupted products (e.g. Condomines et al. 1995; Métrich et al. 2001; Ferlito and Lanzafame 2010 and references therein). Such an evolution tracks the inflow of a new magma type, associated with infiltration of CO_2-rich deep gases in the upper magma storage regions (Spilliaert et al. 2006a; Ferlito and Lanzafame 2010). This enhanced activity has consisted of very abundant gas emissions, persistent Strombolian activity, series of fire-fountains and several fissural eruptions with high effusion rate (e.g. 1991-93; 2001; 2002-2003). In particular, the last twenty years (i.e. after the 1991-93 flank eruption) have been characterized by several series of lava fountain episodes in late 1995 at the NEC and between 1998 and 2001 at SEC. The latter also include the February 1999 eruption, which was fed by a fissure on the SSE flank of the SEC (La Delfa et al. 2001). In particular, the SEC activity shows a periodicity of pre-eruptive magmatic processes, since its reactivation in 1996 up to the onset of 2001 flank eruption, with the alternation of fractional crystallization and mixing between residing and new intruding magma batches, controlled by geometry of the conduit and the balance between refilling magma and erupted lavas. On the contrary, an upper storage system, corresponding to the central conduits region (i.e. depths <100 MPa, Collins et al. 2009), with different size and/or supply rate is hypothesized for the other three summit craters (Corsaro et al. 2013). The post-1970 activity of Mt. Etna has been featured by short but intense periods of explosive activity (e.g. the 2001 July-August eruption), and even of sub-Plinian scale, such as the paroxysmal event on 22 July 1998 at VOR crater. Such a change in the eruptive intensity has to be related to the change in magma composition, initiated during the 1974 flank eruption (Corsaro et al. 2009), with intrusion of a new volatile-rich and more alkali-rich basaltic magma component. This magma component, which has come to play an increasing

ACCEPTED MANUSCRIPT

important role in the plumbing system (see Métrich et al. 2004 and Spilliaert et al., 2006a for details), likely volatile- and Mg-rich (Kamenetsky et al. 2007), is thought to have progressively replaced the trachybasaltic magma formerly residing in the volcano's upper plumbing system, and was first erupted "undiluted" during the 2001 eruption (Métrich et al. 2004). At Mt. Etna, high-energy Plinian eruptions occurred in 3890 BP and 122 BC (Coltelli et al. 1998; 2000). These events, at the same volcano, emphasize the critical role played by the exsolution, separation and expansion of the gas phase from the volatile–rich primitive Etnean magmas, and clearly show that at Mt. Etna fractional crystallization is only one of the processes contributing to the chemistry of magmas. In addition, magma mixing processes can explain both chemical and isotopic variations of the erupted products, as shown for the 1995-2005 activity at Mt. Etna summit craters (Corsaro et al. 2013; Kahl et al., 2015), in which a radiogenic, more primitive but alkali-rich component can be recognized, the one marking the new alkali-rich trend observed at Etna in the last decades. Corsaro et al. (2013) defined the most primitive and radiogenic magma that erupted from SEC during the 17 May 2000 fire fountain, and an evolved, less radiogenic magma emitted on 6 June 1996 during Strombolian activity at NEC, as compositional endmembers 1 and 2 respectively. By choosing such end-members, mixing proportions between end members 2 and 1 can be estimated to vary between 1:0.25 and 1:3 (Corsaro et al. 2013).

2.2 Volatiles (H_2O, CO_2, S and Cl) in Mt. Etna magmas: state of the art.

Several studies based on MI chemistry and volatile contents for past and present Mt. Etna eruptions have been carried out to reconstruct structure and evolution of its plumbing system (e.g., Métrich et al. 2004; Spilliaert et al. 2006a, 2006b; Corsaro et al. 2009; Ferlito and Lanzafame 2010; Figure 1). Generally, H_2O and CO_2 determinations are fundamental to defining *a*) the total (dissolved plus exsolved) volatile content of the parental melt (Papale 2005), and *b*) the depth intervals of reservoirs in which magma evolution takes place (e.g. Moretti et al., 2013a,b; Spilliaert et al., 2006a). On the other hand, S content and speciation state can be used to understand the

ACCEPTED MANUSCRIPT

oxidation state controlling the evolving magma, whereas Cl represents an important tracer to understand the interplay of crystallization and degassing (e,g, Lesne et al., 2011; Spilliaert et al., 2006b) and later stages of volcanic degassing (e.g., Alletti et al., 2009).

Contents of dissolved H_2O and CO_2 up to 3.6 wt% and ~ 3200 ppm, respectively, have been measured in Etna MIs (e.g., Métrich et al. 2004; Spilliaert et al. 2006a,2006b). The very different solubility behavior of these two volatiles indicates that Etnean magmas coexist at depth with a CO_2-dominated fluid phase. Clocchiatti et al. (1992) measured CO_2 concentrations of ~ 98-99 wt% in monophasic fluid inclusions hosted in high-Mg olivines (Fo 92 mol%) from the Mt. Maletto suite (7 ka BP; Condomines et al. 1995), implying that CO_2 is already exsolved at a pressure of 800 MPa, i.e., at a lithostatic depth of about 21-24 km, corresponding to the base of the crust. Large production of CO_2 is testified by the background CO_2 volcanic flux of 4 ktons/day, which was assessed in 1975-1995 (Allard et al. 1991). CO_2 volcanic flux has dropped to 2 ktons/day since 2001 (Aiuppa et al. 2006), but rapidly increases upon replenishment of the shallow magmatic reservoir, yielding values up to ~ 30 times larger, such as in the case of the 2004-2005 effusive eruption (Aiuppa et al. 2006).

High total (exsolved + dissolved) volatile contents have been assessed by Métrich et al. (2004) and Spilliaert et al. (2006a), implying from 1.5 to 8 wt% of CO_2-dominated free-fluid phase in the parental deep magma (calculations based on the Newman and Lowenstern [2002] model). This is in line with the amounts estimated by Scaillet and Pichavant (2005) (up to 5% of free fluid phase) and Aiuppa et al. (2007) (H_2O^{TOT}=3.4 wt%, CO_2^{TOT} = 2wt%; S^{TOT} = 0.32 wt%), based on either experimental data or modeling, the latter by using the Moretti et al. (2003) model updated for the H_2O-CO_2 saturation model of Papale et al. (2006). These high total contents strongly suggest the addition of deep fluids from a devolatilizing slab, infiltrating into the astenospheric mantle that upraises through the slab window over which Mt. Etna has developed (Tonarini et al. 2001).

However, recent simulations of the plagioclase stability fields indicate a large variability in water content within the magmatic system, such that primitive Etnean melts are water-poor

ACCEPTED MANUSCRIPT

(between 1 and 2 wt%) and water enrichment occurs on magma ascent to the surface through fluxing of water induced by decompression and water exsolution at relatively shallow depth, and only subordinately by fractional crystallization (Ferlito et al., 2014; Giacomoni et al., 2014).

Fluxing is typically due to continuous infiltration of CO_2, which promotes magma dehydration through the plumbing system, and the volatile-induced differentiation with consequent enrichment of elements such as alkalis at shallow levels (Allard et al., 2006b; Spilliaert et al. 2006a; Ferlito et al. 2008; Collins et al. 2009; Lanzafame and Ferlito 2010). CO_2 enrichment and H_2O depletion through CO_2 fluxing occur stepwise, but are strongly recognizable in the 140-200 MPa range (Allard et al., 2006b; Spilliaert et al. 2006a; Collins et al. 2009), i.e., at nearly isobaric conditions. Fluxing allows the residing magma to re-equilibrate under different total volatile contents of H_2O and CO_2 (Barsanti et al. 2009). The involved CO_2-rich gas phase can be purely magmatic, separated at great depth (e.g., Clocchiatti et al., 1992), or/and external and derived from decarbonation of the thick limestone platform present in the basement of Mt Etna at a depth > 4 km b.s.l. (Lentini et al. 1982; Spilliaert et al. 2006a). The carbon isotope composition of the volcanic gas (Allard, 1986; Chiodini et al. 2011; Paonita et al., 2012; Rizzo et al., 2014) indicates that pre-1990 samples had somewhat lower $\delta^{13}C$ (~ -3‰ vs PDB) than post-1990 samples (between -2 and -1 ‰ vs PDB), which may reflect a change in the source of gas supply. Such a change could be consistent with either (a) interaction with carbonate in the basement, or (b) increased mantle metasomatism by slab-derived carbon-rich fluids (Tonarini et al. 2001). However, important $\delta^{13}C$ variations are intrinsic in the short-term magmatic activity of Mt. Etna. Measurements of CO_2/SO_2 and of $\delta^{13}C$ in CO_2 were carried during the 2014 activity and show that both indicators are concordant, revealing that early degassing of CO_2 may lead to peaks in both values and produce the highest $\delta^{13}C$ values ever measured at Etna (1.5 ‰) (Rizzo et al., 2015). These results, in conjunction with the study of noble gas isotopes and abundances also confirm the occurrence of mixing between fluids exsolved at different depths in the magmatic system (Paonita et al., 2012).

ACCEPTED MANUSCRIPT

Sulfur is a sensitive tracer to investigate volcanic evolution to eruptions (Oppenheimer et al., 2011) and its speciation between SO_2 and H_2S in the gas phase reflects the physico-chemical conditions of magmas feeding eruptions (e.g., Moretti and Papale 2004; Burgisser and Scaillet 2007). Based on the composition of magmatic gases discharged from Etna volcano in July 1970 (Huntingdon 1973, Gerlach 1979), in 1975-1976 (Allard 1986), in April 1983 (Le Guern 1988) and presently (Aiuppa et al. 2005, 2006), SO_2 is the prevalent sulfur gaseous species at surface conditions. The SO_2 flux has traditionally been measured by using UV spectroscopy, yielding to a long-term time-average value of ~5,000 t/d with peaks to 25,000 t/d during eruptions and a large excess degassing rate of S compared to solid magma in the long term (Allard, 1997; Burton et al. 2004 for a review). Chlorine emissions, which are sourced by shallow (<50 MPa, Spilliaert et al. 2006a, b) degassing, average at ~1,000 to 2,000 t/d, although SO_2/HCl proportions in the plume have been seen to vary substantially over time, and from one crater to another (Aiuppa, 2009).

3. Samples, Analytical Procedures and Results

An olivine-hosted MIs study was performed on scorias extruded during the 1997-98 BN Strombolian eruption, during the paroxysmal event of February 1999 from the SEC (La Delfa et al. 2001), and from products of the 122 BC Plinian eruption (Coltelli et al. 1998). Olivine crystals were handpicked under binocular microscope, from the 0.5-1 mm fraction, after gentle grinding and sieving. Because of rapid cooling of scoriae upon eruption, MIs were preserved as glass. Only in few cases they are-bubble free, and most often they display one bubble. The bubble/MI volume ratio does not appear constant and is highly variable, suggesting an heterogeneous trapping of a saturated magma (e.g., Spilliaert et al., 2006b). However, no attempt was made to determine if these are shrinkage bubbles (and therefore empty) or if they contain a CO_2- or H_2O-rich fluid phase.

Visually observed sulfide globules (Figure 5) are often associated with intergrowth of olivine and oxides, mostly (but not only) in the low-forsterite olivines.. They are typical of samples

ACCEPTED MANUSCRIPT

characterized by low sulfate proportions (Moretti et al., submitted) and were also found in clinopyroxene and plagioclase crystals..

We just provide here a summary of the conditions used for minerals and MIs analyses, whereas the details of the analytical procedures are provided in **Appendix**. Major elements, chlorine, phosphorous and sulfur concentrations in MIs were measured by electron microprobe (EMP) CAMECA-SX 50 (CAMPARIS Jussieu, France). Major elements in melt inclusions were analyzed with 10 nA beam current, 10 mm spot size, and counting time of 10 to 25 s. Sulfur, chlorine and phosphorus analyses were carried out with 30 nA beam current, 15 mm spot size, counting times of 100 to 200 s. Analytical uncertainties were 3.5% for Si, Al, Mg, Fe, Ca, K and Na, and 5% for Cl, S and P.

On a subset of doubly polished MIs (see **Appendix** and **Supplementary Material**), Infrared Spectroscopy measurements of dissolved H_2O and CO_2 were carried out prior to any other analysis, by using a NICOLET® Magna 550, associated to a microscope Spectra-Tech® IR-plan. Errors are 10% for H_2O and at most 25% for CO_2. We have of course discarded inclusions lying on cracks, such that presented data and their processing were not affected by bubble decrepitation yielding CO_2-loss from the inclusions during ascent (MacIennan 2017)

3.1 Melt inclusion chemistry and volatile contents

A total of 50 olivine phenocrysts (forsterite content ranging from 69 to 82 mol %; see **Supplementary Material**) were selected for studying MIs fully enclosed in their host crystal and embayments still in contact with their surroundings. Figure 2 reports the Total-Alkali-Silica classification diagram (TAS; Le Maitre 1979). Only for this diagram, compositions have been normalized to 100 wt% on a volatile free basis, in order to compare them with whole rocks. MIs from SEC and BN (1999 and 1997-98 respectively), are K-trachybasalts and K-basaltic trachyandesites displaying a strong tephritic affinity. Those from products of the 122 BC eruption fall in the field of intermediate terms of alkaline series, which are ascribed to trachybasalts and

ACCEPTED MANUSCRIPT

trachybasaltic andesites. Because of their sodic affinity they may be classified as hawaiites or as hawaiites and mugearites.

Olivines in the analyzed products show forsterite (Fo) contents ranging from 69 to 83 mol.%, (Fig. 3). All the Fo range is recorded in the BN and SEC products, whereas the majority of olivine crystals from samples of the 122 BC eruption have Fo contents in the 74 to 83 mol % range. All these olivines entrap MIs characterized by highly variable volatile contents (H_2O from 0.19 a 3.5 wt.%,, CO_2 from 81 a 1833 ppm, Cl from 0.05 a 0.46 wt.%, S from 0.017 a 0.39 wt.%). Because the highest Fo values are generally associated with the highest volatile contents (except for Cl), the data are consistent with degassing accompanied by crystallization, although the free exchange of crystals among different magma batches due to the occurrence of mixing/mingling processes cannot be discarded.

The occurrence of magmas differently enriched in potassium emerges from diagrams in Figure 4, in agreement with previous studies (Metrich et al. 1993; Corsaro et al. 2009, 2013). An offset in K_2O vs Na_2O, K_2O vs P_2O_5 and K_2O vs Cl (Fig. 4a-c) occurs between 122 BC and recent products. H_2O, CO_2 and S contents versus K_2O have been plotted in Figure 4d-f showing the peculiar enrichment in H_2O and CO_2, but not S, of low-K products. H_2O and CO_2 are generally negatively correlated with K_2O, indicating degassing coupled to crystallization. However, this occurs along multiple paths and is complicated by variable degrees of potassium enrichment, particularly evident in the K_2O vs H_2O diagram (Fig. 4d). The negative correlation with K_2O is less evident for sulfur, especially because low-K_2O MIs from the 122 BC Plinian event show lower sulfur contents (S < 2000 ppm) than those from the other analyzed products (Fig. 4f).

As a whole sulfur concentrations vary from ~ 250 to > 4000 ppm, whereas chlorine contents vary from 500 to 4600 ppm over a wide interval of chemical differentiation (Fig. 3). MIs from the BN 1997-98 and SEC February 1999 eruptions encompass the same range of sulfur, chlorine and H_2O contents (S ≤ ~2500 ppm, 1000 < Cl < 4600 ppm and H_2O ≤ ~ 1.2 wt%), but few MIs from BN 1997-98, although hosted in a Fo_{80} olivine, are characterized by the highest observed values of

ACCEPTED MANUSCRIPT

dissolved sulfur (S~ 4200 ppm wt). The low K_2O (~2 wt%), P_2O_5 (0.59 wt%) and high CaO/Al_2O_3 ratio (0.7) of these samples reflect the primitive nature of these MIs.

Being melt inclusions all from scoriae and explosive products, they were rapidly quenched upon eruption, preserving the volatile content of their pre-eruptive carrier melt (Hartley et al., 2015). As a matter of fact, MIs show a sharp contact with surrounding olivines. This indicates a very rapid cooling, which inhibited further exchanges between the melt droplet and the host crystal. We discount full re-equilibration between melt and olivine after entrapment. If post-entrapment crystallization (PEC) occurred, it is negligible (see **Appendix**). Therefore, in the following elaborations we will use directly analytical data.

Similar considerations apply also to sulfides (Figure 5). Etnean magmas are generally FeS undersaturated, but may reach saturation under conditions in which sulfide separation would be driven by magma differentiation (Scaillet and Pichavant, 2005; Marini et al., 2011). Such an evolution is confirmed by Spilliaert et al. (2006b), who report sulfide globules in the samples from lava fountains of the 2002 flank eruptions. We discard the possibility of sulfide saturation as a post-entrapment phenomenon within the inclusions. PEC being negligible (see **Appendix**), its eventual effect on S-concentration would be minor and unable to explain the presence of the episodically observed sulfides. Considering that stoichiometric pyrrhotite (density 2700 kg/m^3) contains 365,000 ppm of sulfide, if one restores S-rich (> 2000 ppm) melt inclusions for the amount of sulfide contained in a globule occupying only 0.5% of the inclusion volume, unrealistic pre-entrapment concentrations (> 5,000 ppm) would be attained. This cannot be obtained via PEC at the scale of the single MI. Therefore, sulfides unmixed/precipitated as primary phases and were episodically trapped by MIs in virtue of their nugget effect concentrating sulfur, resulting in apparent extremely high local concentrations of sulfur.

4. Data Analysis and modeling

ACCEPTED MANUSCRIPT

4.1 Estimates from H_2O-CO_2 data: pressure-depth and total volatiles

The new H_2O-CO_2 data provided in this study (**Supplementary Material)** are plotted on saturation isobars (Fig. 6a) drawn with the Papale et al. (2006) model, for a temperature of 1200°C, which is close to the 1220°C value of Kamenetsky et al. (2007) for deep volatile-rich Etnean magmas. Note that this temperature is only 10% greater than temperatures recorded by lavas extruded at surface vents (close to 1090°C) during the February 1999 eruption (La Delfa et al. 2001). Maximum entrapment pressure was computed at ~300 MPa for MIs from crystals hand picked from the February 1999 sample, and agrees well with previous results available in the literature (Fig. 6a**)**.

Although we did not analyze H_2O and CO_2 contents by FTIR on the majority of MIs entrapped in primitive olivine crystals from products of the 122 BC eruption, literature data on products from this and from similar Plinian eruptions, such as the 3930 BP event (Coltelli et al. 2000; Del Carlo and Pompilio 2004; Kamenetsky et al. 2007), are characterized by H_2O and CO_2 contents up to 4 wt% and 4000 ppm, respectively, yielding the highest MI entrapment pressures (~ 500 MPa) and showing that volatile-rich Etna magmas can be found at depths > 15 km, at least) (Fig. 6a).

Particularly for the low soluble CO_2 component, dissolved contents are not representative of total abundances, given by the presence of an exsolved gas phase, in which H_2O and CO_2, represent more than 95 %. Especially at depth, these two components approximate the totality of such an excess gas phase (e.g., Moretti et al., 2003). On the saturation isobar diagram (Fig. 6a), each pair of H_2O-CO_2 dissolved in MIs can be produced by a virtually infinite number of degassing trends, depending 1) on the presence and relative amount of the initial gas phase, hence total (exsolved+dissolved) H_2O and CO_2 volatile abundances (H_2O^{TOT} and CO_2^{TOT}), and 2) the degassing style (closed-system, open-system, or a combination of both). As a rule of thumb, it is considered that the closed-system degassing trend crossing the rightmost datapoints on a H_2O-CO_2 saturation isobar diagram well approximates the total volatile abundance of the system (e.g., Métrich et al.,

ACCEPTED MANUSCRIPT

2004; Spilliaert et al., 2006a; Arienzo et al., 2010; Moretti et al., 2013b). The curvature of such a trend around the 200-100 MPa region, where the contrast of H_2O and CO_2 solubilities is such that H_2O starts exsolving significantly and little CO_2 stays dissolved above typical detection limits for such a component, is greatly controlled by H_2O^{TOT} and especially CO_2^{TOT}.

In Figure 6a, we see that the bulk of data can be bounded by a closed-system degassing trend characterized by high total volatile contents (H_2O^{TOT} = 4 wt%; CO_2^{TOT} = 2wt%), such that CO_2^{TOT} is up to ten times more abundant than the largest dissolved amount measured in a SEC 1999 MI, and ~5 times larger than highest dissolved contents from literature data. These values are in line with earlier determination of Scaillet and Pichavant (2005) and consistent with those of Aiuppa et al. (2007). On their left side, datapoints are limited by a gas buffered trend (gas/melt mass ratio ~ 0.3) for a molar $CO_{2(g)}/H_2O_{(g)}$ ratio of 5. This trend, which involves low-density magmas basically unaffected by degassing because buffered by the exsolved volatiles, is in good agreement with same trends observed from Stromboli K-basaltic MIs (molar $CO_{2(g)}/H_2O_{(g)}$ >3; Pino et al., 2011), latitic and trachytic MIs from Campi Flegrei (molar $CO_{2(g)}/H_2O_{(g)} \approx 4$; Mangiacapra et al., 2008; Arienzo et al., 2010), and particularly K-trachybasaltic MIs from Ischia (molar $CO_{2(g)}/H_2O_{(g)} \approx 5$; Moretti et al., 2013b).

This evidence of a CO_2-rich gas phase already exsolved at large depth can be detailed by using the method described in Papale (2005), focusing on the H_2O-CO_2 pair dataset acquired in this study. Following this author, we generated the total volatile (TV) lines, which represent the locus of total volatile contents consistent with the amounts dissolved in the liquid and measured in MIs (Fig. 6b). Each TV line is generated by imposing different relative amounts of melt and gas phase and by calculating the H_2O-CO_2 gas phase composition required to reproduce the (dissolved) H_2O-CO_2 pair. Uncertainties in the procedure are then essentially related to the adopted melt-gas saturation model.

Along a TV line, the gas/melt ratio varies progressively, from zero (*total contents = dissolved contents*) to infinite (gas-dominated conditions) (Fig 6b). In case of an ideally closed degassing

ACCEPTED MANUSCRIPT

system, all TV lines generated from dissolved H_2O-CO_2 pairs must converge to the same point, representing the total volatile content of the system (Fig. 6b inset). In case of gas separation during the degassing process (open-system conditions) TV lines will not converge to one common point.

Therefore, in Figure 6c, points where TV lines cross identify H_2O^{TOT}-CO_2^{TOT} pairs that represent the total volatile contents for the considered samples. In particular, primitive MIs from the February 1999 and 2001 activity generate TV lines (solid lines) crossing at several H_2O^{TOT}-CO_2^{TOT} pairs, revealing that a quite complex degassing history and style also affects the deep magmatic system. Line intersections give values from 3.4 to 3.8 wt % (for H_2O^{TOT}) and 1.9 wt% (for CO_2^{TOT}), which best represent the initial concentrations in February 1999 parental melts. In the shallower portions of the plumbing system, the magma is characterized by larger CO_2^{TOT}/H_2O^{TOT} ratios: note, for example, the two intersections at [$H_2O^{TOT} \approx 2\%$; $CO_2^{TOT} \approx 4.7\%$] and [$H_2O^{TOT} \approx 2.3\%$; $CO_2^{TOT} \approx 1\%$], which clearly show CO_2 addition due to fluxing through the plumbing system (e.g., Spilliaert et al., 2006a; Aiuppa et al., 2007) and identify local reservoirs where CO_2-rich magma is stocked (Paonita et al., 2012). We then identify two possible fluxing arrays (arrows in Fig. 6c) qualitatively embracing all possible paths: *a*) CO_2-gain (increasing CO_2^{TOT}) and dehydration (left red arrow) and *b*) constant CO_2^{TOT} and dehydration (cyan arrow). Note that the reverse evolution of the magma system along such paths is not possible (unless reversing the pressure gradient) but could explain why some authors also refer to H_2O fluxing throughout the Etna plumbing system (Ferlito et al., 2014).

Despite the availability of only two H_2O-CO_2 pairs, conditions of important CO_2-enrichment are recorded by BN 1997-98 activity, yielding very high CO_2^{TOT}/H_2O^{TOT} (mass) ratios and crossing at $CO_2^{TOT}/H_2O^{TOT} \approx 20$ (dashed lines; Fig. 6c), a value consistent with the trend bordering datapoints on the left side of Fig.6a.

TV lines relative to MIs in crystals from the 122 BC Plinian samples do not allow inferred total volatile contents consistent with those of February 1999 and 2001 products. In fact, we miss intersection points, and TV lines depict a divergent fan, especially if we include the data from Del

ACCEPTED MANUSCRIPT

Carlo and Pompilio (2004) (dashed lines in Fig 6d), which reveals the onset of complex patterns of either gas loss or gain in open system conditions. With respect to MIs from recent activity, TV lines generated by 122 BC MIs are shifted toward lower CO_2^{TOT}/H_2O^{TOT} ratios, with four of them collapsing along the abscissa, which suggests important CO_2- loss. On the other hand, a few of them (five) are steep and reveal dehydrated and CO_2-rich conditions: they approach the highest CO_2^{TOT}/H_2O^{TOT} ratios observed for BN 1997-1998 MIs, reflecting extensive CO_2 fluxing and addition producing the gas-buffered trend in Fig. 6a.

The never crossing TV lines generated from 122BC MIs could be compatible with H_2O-fluxing (Ferlito et al., 2014), superimposing to previous CO_2-fluxing. Water fluxing, may have occurred in the shallow ($P \leq 150$ MPa; Figure 6a) part of the 122 BC plumbing system, in response to exsolution of the highly soluble water component. This could have produced the flattening of CO_2^{TOT}/H_2^{TOT} lines on the H_2O-rich side of Figure 6c.

Therefore, 122 BC samples display peculiar features of the extensive open-system degassing occurred at large depth: the magmatic system, first, got rid of its CO_2, fluxing the shallower system but without accumulating in intermediate magma storage zones like those observed throughout the plumbing system of recent activity; secondly, subsequent water exsolution and fluxing in the shallow system ($P \leq 150$ MPa) occurred, as recorded by TV lines.

This may suggest that the set of total volatiles, particularly CO_2^{TOT}, inferred for recent products may not be fully representative of the initial volatile content of the primitive magma: instead, it may represent an intermediate accumulation level resulting from fluxing of CO_2 released from an even deeper but unsampled pristine source at the roots of the Etnean system. However, for the purposes of this study, and in agreement with Aiuppa et al. (2007), we will retain $H_2O^{TOT} \approx 3.5$ wt% and $CO_2^{TOT} \approx 2$wt%.

We must here remark that analytical uncertainties on H_2O and CO_2 would make each TV back-calculation a field rather than a line, so intersections would correspond to vast polygonal areas spreading over a wide range of H_2O^{TOT} and CO_2^{TOT} values. However, our goal is not the

ACCEPTED MANUSCRIPT

identification of all populations of total volatiles needed to fit the whole MI database (e.g., Barsanti et al., 2009). Rather, we want to highlight the trends of either CO_2- and H_2O-fluxing and identify the total volatile contents that define a plausible initial pole for the parental magma.

4.2 Sulfur release and the role of gas fluxing

Figures 7a,b report the S-H_2O covariation and degassing trends from a region (labeled IP) of dissolved volatiles in which H_2O is about 3.0 wt% (in agreement with Figure 6) and dissolved sulfur is about 0.35 wt%. The IP region corresponds to a significant cluster of datapoints of the highest measured values of sulfur and lowest K_2O contents (~2.2 wt%) (Figure 4 and **Supplementary Material**). We use the model of Moretti et al. (2003) for C-H-O-S-silicate melt equilibrium to numerically reproduce the different possible degassing trends running across measured datapoints. The model couples the sulfur solubility model of Moretti and Ottonello (2003a,b; 2005), which also returns the speciation state of S between S^{2-} and SO_4^{2-} (Moretti et al., submitted), with the H_2O-CO_2 saturation model of Papale et al. (2006). Model adoption confirms that H_2O and S concentrations in the IP region are in consistent with initial dissolved volatile abundances computed for a set of total volatiles (H_2O^{TOT} = 3.5 wt%; CO_2^{TOT} = 2 wt%; S^{TOT} = 0.35 wt%) that are in line with those already used in Aiuppa et al. (2007). However, the spread within IP region may also be determined by the infiltration of volatiles (essentially CO_2) released from the unsampled and deeper primitive magma.

Two reasonable equilibrium approaches can be followed to reproduce analytical data. 1) Using selected total volatiles, degassing trends are all generated within the IP for different redox states ($-3 \leq NNO \leq 3$; Figure 7a). In this case, measured datapoints are embraced by model-generated trends, whose curvature and varying slopes reflect variations of the redox state. 2) Processes other than degassing occur, such as gas (CO_2)-fluxing and/or the precipitation of an immiscible sulfide-bearing phase (Figure 7b), in agreement with visual observations (e.g., Fig. 5). These additional processes alter the total amount of dissolved volatiles, shift the beginning of degassing trends outside the IP,

ACCEPTED MANUSCRIPT

to other starting conditions that are depleted in H_2O or S, and allow generating the many possible degassing trends which match analytical data.

Although the possibility that the redox state of a magmatic system is highly variable, the former approach returns unrealistic results. First, it is not possible to generate with selected total volatiles a reduced degassing trend from the IP able to cross data at $H_2O \geq 2.5$ wt% and $S \leq 0.35$ wt%. Second, and more important, oxidized trends crossing through high-S and low-H_2O datapoints (e.g., NNO +2 or +3; Figure 7a) are characterized by sulfur dissolved as sulfate (SO_4^{2-}), which is incompatible with both speciation data (Moretti et al., submitted) and the visual occurrence of sulfide globules (Figure 5).

We then choose the second approach, that is, a combination of degassing trends plus FeS separation and CO_2-fluxing. Simulations in Figure 7b are presented for $\log fO_2$ at NNO, in agreement with Aiuppa et al. (2007, 2011). However, they are unaffected by $\log fO_2$ variations of ± 0.5 log units, that is, within one log unit. In all cases, degassing trends are almost rectilinear, particularly Tr1, Tr2 and Tr3, suggesting that sulfur and H_2O have similar solubilities under these fO_2 conditions (Fig. 7b).

The effect of CO_2 addition, due to fluxing, on the shift of H_2O-S degassing patterns is accounted for by trend Tr2, which shifts Tr1 to Tr3 and well explains the largest extent of dehydration displayed by BN 97-98 and CSE 1999 MIs (Fig. 6b,7b). Along Tr2, sulfur, contrary to H_2O, is retained and concentrates instead within the MIs. This array interpolates the starting poles of the many possible degassing paths (such as Tr3) that commence from progressively dehydrated melts because of fluxing or a combination of fluxing plus self-mixing between deep volatile-rich and degassed magma portions. The fluxing array (Tr2) ends and the degassing trend Tr3 starts- at 140 MPa, where a major discontinuity and magma ponding zone has already been inferred (Métrich et al., 2004; Ferlito et al., 2014; see also Figure 6a).

Trends Tr4 and Tr4bis (Fig. 7) start from relatively H_2O-rich and S-depleted contents (here taken at 3.2 wt % and 1300 ppm for Tr4, and 3.2 wt % and 2300 ppm for Tr4bis) which may be

ACCEPTED MANUSCRIPT

obtained only after an early FeS separation (Tr5) (Marini et al., 2011). This may have taken place in the early 122 BC magma, causing depression of the dissolved S content from the original total value (~ 3500 ppm; Figs. 3 and 4), as also discussed in a companion paper (Moretti et al., submitted).

Finally, the arrow labeled Tr6 within the initial pole (IP) domain (Fig. 7) represents the H_2O-S pattern followed by Etnean primitive melts that started crystallizing at depth, initially concentrating H_2O and S when degassing is dominated by CO_2 exsolution (see also Marini et al., 2011). Therefore, early exsolution of a CO_2-rich gas, due to crystallization at depth, fluxes the upward magma and allows retaining contents of soluble H_2O and S up to 3.5 wt% and 0.45 wt%, respectively, embodying highest values measured in MIs (**Supplementary Material** and Figure 3). Note that the adoption of H_2O^{TOT} and CO_2^{TOT} of 4 wt% and 2 wt%, respectively (see the bounding degassing trend in Fig. 6a), and S^{TOT} of 0.41 wt% (highest measured dissolved S content; **Supplementary Material** and Fig. 3), could be alternative to Tr6 within the error limits for S contents and would shift the IP toward the upper right corner of Figure 7b, that is at a higher starting pressure. This would not impact appreciably on trends departing from the IP (Tr1, Tr2 and Tr5).

The different behaviors displayed by H_2O-S co-variations corroborate a view in which the magmatic system is parceled in different portions with variable total volatiles, reflecting the effect of CO_2 fluxing (Spilliaert et al., 2006a) and in agreement with the model of mixing of fluids exsolved at various depths developed by Paonita et al. (2012) on conservative components such as CO_2, Ar and He.

4.3 The role of crystallization and gas fluxing on chlorine release

The behavior of chlorine reflects the high solubility of this component in Etnean melts, which explains the constancy of chlorine concentration throughout chemical differentiation (Fig. 4c). Although most chlorine tends to degas at shallow pressure, hence depth, its solubility behaviour depends on the relative H_2O/CO_2 ratio in the gas phase (Alletti et al., 2009). We then used equation

ACCEPTED MANUSCRIPT

3 in Alletti et al. (2009) [$D_{Cl}^{f/m} = 12.732 \times P^{-0:0853}$; P in MPa] to introduce a P-dependent chlorine partition coefficient between gas and melt ($D_{Cl}^{g/m}$) in the frame of the Moretti et al. (2003) and Moretti and Papale (2004) approach. Moreover, we also included the role of crystallization: a maximum crystallization of 67 wt% can in fact be evaluated on the basis of variations recorded by the P_2O_5 component (from 0.5 to 1.5 %; Fig. 4b), considering P_2O_5 as an incompatible component (apatite not on the liquidus; see also Spilliaert et al., 2006b), such that $\%\,\text{crystals} = 1 - \frac{[P_2O_5]^{IN}_{wt\%}}{[P_2O_5]^{FIN}_{wt\%}}$.

Figure 8 reports closed-system (solid lines) and open-system (dashed lines) degassing trends on the H_2O-Cl diagram. Model simulations are for open-system decompression and degassing from 400 MPa. Crystallization was accounted for by adopting the following empirical P-dependent linear behavior, similar to eq. 56 in Marini et al. (2011), such that crystallization is zero at at 400 MPa and the maximum values, 67 wt%, is reached at 0.1 MPa:

$$\%\ \text{crystals} = -3.17 \times P(\text{MPa}) + 67.32 \qquad (1)$$

To model the difference in Cl contents between recent products and those from the 122 BC Plinian event, trends must necessarily shift. The simplest hypothesis is assuming initially different Cl^{TOT}, which would be higher for the 122 BC magma. It is in fact well known that the pre-1970's magmas are richer in Cl with respect to the present-day magmas (Corsaro and Métrich, 2016). Degassing trends are drawn for initial CO_2^{TOT} of 2 wt%, H_2O^{TOT} varying from 3.5 wt% (recent products) to 4 wt% (122 BC), and Cl^{TOT} = 2300 ppm (recent products) and 3500 ppm (122 BC). It is worth noting that saturation properties require chlorine to be already exsolved at large depth in the CO_2-dominated gas phase. However, Cl-exsolution is very little, close to zero, for 122BC, such that the Cl-dissolved content corresponds to the total one at 400 MPa (Figure 8). In the case of the recent products, deep Cl-exsolution amounts to 500 ppm, that is, the difference between Cl^{TOT} and the dissolved amount at ~350 MPa (1800 ppm; Figure 8). In agreement with the experimental evidences of Alletti et al. (2009) on Etna samples, this deep exsolution is likely due to the high amount of exsolved CO_2 at depth. Differences in H_2O^{TOT} do not appear to appreciably affect the Cl-

ACCEPTED MANUSCRIPT

H_2O evolution path, such that trends for H_2O^{TOT} at 3.5 wt% and 4 wt% overlap within uncertainty (see paragraph 4). Both systems exsolve chlorine progressively while depressurizing (solid lines). When crystallization is considered, strong Cl-enrichment can be modeled. An important event of crystallization occurs in fact at shallow depth (P ≤ 20 MPa, i.e., H_2O < 0.5 wt%) for both systems (122 BC and recent products), determining a change in slope in H_2O-Cl trends (Fig. 8), and leading to increasing Cl contents. It is worth stressing here that, for each system, closed-system and open-system degassing paths overlap until crystallization takes place. In case of recent products, low-P data are best embraced by a simple closed system degassing trend in absence of crystallization and an open-system degassing trend in presence of crystallization. In case of 122 BC, a simple closed-system degassing trend, in presence of crystallization, matches well with available data.

The major feature emerging from simulations is then the difference in Cl^{TOT} between 122 BC and recent products, which needs alternate explanations. One could be the involvement of different magma sources for 122 BC and recent activity, possibly complicated by mixing phenomena (e.g., Corsaro et al. 2009, 2013). Some high chlorine concentrations can in fact be found in products from the recent activity that seem to pursue the 122BC trend at relatively high K_2O values (Fig. 4). However, crystallization may easily account for the Cl-enrichment of these MIs, most of which cannot be reported in Fig. 8 as they lack the determination of H_2O. Moreover, involvement of magmas from two different sources and their mixing does not afford the basic question: how to switch from the relatively Cl-rich, K-poor (or Na-enriched) 122 BC source to the relatively Cl-poor, K-rich (or Na-enriched) source of recent products ?

The alternate explanation is suggested by the experimental work of Alletti et al. (2009), reporting that the introduction of CO_2 in the system tends to diminish $D_{Cl}^{g/m}$. Therefore, CO_2-fluxing can operate a significant switch in chlorine contents, from a 122 BC-like parental melt to a term corresponding to that involved in recent activity. Two fluxing lines (one for a pure CO_2 gas, the other for a gas with H_2O=5 wt% and CO_2 = 95 wt%) are modeled in Figure 8, which allow the deep transition from the 122 BC trend (H_2O^{TOT} = 4 wt%; CO_2^{TOT} = 2 wt%; Cl^{TOT} = 3500 ppm) to

ACCEPTED MANUSCRIPT

that of recent products (H_2O^{TOT} ≈3.5 wt%; CO_2^{TOT} ≈ 2 wt%; Cl^{TOT} = 2300 ppm). Such a transition is modeled by extracting 20 wt% of gas phase and adding a corresponding amount of fluxing gas at each computational step corresponding to 5 MPa of depressurization. This produces a progressive CO_2-enrichment and dehydration, and also depresses the dissolved chlorine content at concentration levels that at P < 350 MPa (Fig. 6a) are close to those typical of the basic trend for recent products, Cl^{TOT} = 2300 ppm.

5. Discussion

5.1 Total volatiles and the shift of volatiles release patterns

Measured volatile abundances suggest a polybaric evolution of the Etnean system, in which simple paths of degassing and crystallization cannot be easily distinguished due to gas infiltration and magma mixing. Complex degassing behaviors are seen, particularly in case of highly soluble and reactive components, such as sulfur and chlorine (Fig 4). Such a complexity could reflect mixing processes, whose occurrence can partly explain the chemistry of BN and SEC products from recent activity. The observed variations (Fig. 4) can in fact result from self-mixing between i) the same volatile and K-rich end-member, which became substantial from 1999 to 2000 (Corsaro et al. 2013) and is best represented by aphyric primitive products erupted during 2002–2003 (Spilliaert et al. 2006a; Corsaro et al. 2009), and ii) its degassed and more evolved products. Self-mixing would also explain the presence of the whole spectrum of MIs in the Fo_{80-70} olivine range (Fig. 3). Also the offset between 122 BC and recent products in K_2O vs Na_2O, K_2O vs P_2O_5 and K_2O vs Cl plots (Fig. 4a-c) can be given by mixing processes superimposing to the normal trend of fractional crystallization (Metrich et al. 1993; Corsaro et al. 2009, 2013).

However, self-mixing alone cannot justify the existence of clearly fluxed magma portions (Fig. 6a) and the occurrence of variable intersection points in Figure 6c, characterized by variable amounts of H_2O^{TOT} and, particularly, CO_2^{TOT} which suggest a complex evolution of the Etnean

ACCEPTED MANUSCRIPT

magmatic system, due to gas addition or loss (Spilliaert et al. 2006a; Collins et al. 2009; Paonita et al., 2012). The set of total volatile contents in the parental magma (P > 400 MPa) have been identified at about 4 wt% and 2 wt% of H_2O^{TOT} and CO_2^{TOT} on products from the 3890 Plinian BP eruption and recent products (Fig. 6a and 6b; Kamenetsky et al., 2007). Magma parcels with total volatile contents even exceeding those of the parental melt have been recognized from products of the recent activity (Fig. 6b), revealing that a large role is played by CO_2 addition throughout the plumbing system, which is characterized by intervals in which large amount of volatiles are stocked. This evidence, which does not exclude self-mixing processes of the magma batches, is surely reminiscent of the mixing model of fluids released at different depths proposed by Paonita et al. (2012). On the other hand, products from the 122 BC Plinian eruption depict a somehow different scenario, in which open-system degassing and continuous gas extraction takes place since the deep parental magma region. The consequent lack of crossing TV lines does not allow to definitely constrain total volatiles for the 122 BC (Fig. 6c Papale, 2005), which are considered to be the same as for recent activity and the analogous 3890 BP eruption (Fig. 6a,b).

Our simulations (Figs. 6, 7, and 8) have shown that CO_2 fluxing greatly determines the evolution of the other measured dissolved volatiles, in combination to crystallization (e.g., Fig. 7). In case of sulfur, modeling has demonstrated that CO_2-fluxing may shift total volatile abundances producing the initial trends that on the H_2O-S diagrams run through measured datapoints (e.g. trend Tr2 in Fig. 7b). However, our simulations were conducted by investigating melt-gas equilibria, independently of the presence of a FeS-bearing phase, either solid or liquid. Thus, it is not immediate to reconcile the presence of sulfide globules with high-S concentrations in such melts fluxed by CO_2, because the S-budget of the whole trapped system (MI + sulfide globule) largely exceeds the value of S^{TOT}. The effect is particularly evident for CSE 1999 and, particularly, BN 1997-98 MIs that fall on Tr2 and Tr3 trends, and show the largest extent of CO_2-fluxing and consequent dehydration (Fig. 6b). In these dehydrated MIs, sulfur, contrary to H_2O, is retained and concentrates instead within the MIs, reaching high values despite the presence of sulfide globules

ACCEPTED MANUSCRIPT

(e.g., sample d9 from the BN 1997-1998 dataset; **Supplementary Material**) that concentrate large amounts of S. However, the presence of sulfide globules determines a "nugget" effect, such that the amount of sulfur in the sulfide globule plus the sulfur dissolved in the melt may not be representative of the actual S-budget within the volume of the trapped MIs, but of total sulfur in a much larger equilibrium volume. In such a case, trapped MIs carrying a sulfide globule have an apparently extremely high S-budget (dissolved sulfur in melt, plus sulfur in the sulfide globule) which instead should be distributed over the much larger but unconstrained equilibrium magma volume which includes also MIs not displaying sulfide globules.

Consequently, high S-budgets of some MIs may either reflect 1) unexpectedly high sulfur abundance inherited from the deep parental source or, 2) combination of multiple crystallization, increasing the S-content of the residual melt, and nugget effect by precipitating sulfide globules in a magma whose patchy distribution of sulfur is being recorded by MIs entrapment. CO_2-fluxing, yielding dehydration and consequent crystallization (e.g., Blundy and Cashman, 2008), clearly relates to the second case, as testified by the sulfide-bearing BN 97-98 MIs compositions, more evolved than the sulfide-lacking 2001 ones.

Also Marini et al. (2011), in their modeling of sulfur isotopes ($\delta^{34}S$) from Etnean volcanics, highlighted the two above possibilities. Starting from an initial mantle value ($\delta^{34}S$ = 0 ‰ vs CDT), they were in fact able to model measured $\delta^{34}S$ values assuming an early trend of FeS separation, and showed that that the same initial condition for fractionation patterns of $\delta^{34}S$ can be obtained either by starting from a parental melt with S ≈ 1.1 wt% from which only FeS precipitates, or by allowing the CO_2-rich parental melt (with S^{TOT} = 0.32 wt%) to degas and crystallize. Based on their independent findings, early degassing at depth is likely to lead to S (and also H_2O) enrichment, similarly to Tr6 in Figure 7, unlike FeS separation (Marini et al.,2011). CO_2 exsolved in such an early degassing stage fluxes the magma ponding upward at lower pressures, and according to our simulations (e.g., Tr2, Fig. 7b), makes the melt a sort of repository of the highly soluble S component, thus preventing its loss.

ACCEPTED MANUSCRIPT

On the other hand, trend Tr5 (Fig. 7b), along which degassing trends such as Tr4 and Tr4-bis start taking place, can be explained by simple separation of FeS from IP, which in absence of CO_2-fluxing, determines S-depletion in the melt. Sulfide separation would require the onset of more oxidized conditions along Tr5 proportional with the removal of S^{2-} and Fe^{2+}, which make up the FeS separated phase, thus yielding high residual proportions of Fe^{3+} and SO_4^{2-} in the residual melt. This is confirmed by the large amount of S as sulfate from XANES analyses of hydrous ($H_2O \geq 2.5$ wt%) MIs from 2001 eruption. (Moretti et al., submitted).

Summarizing, earlier separation of sulfide globules can affect the IP and its sulfur total content. Sulfide separation may occur in absence of CO_2 fluxing (Tr5), substantially resulting in the depletion of the melt S-content (Tr5). On the contrary, in presence of CO_2 fluxing (Tr2), the melt retains high concentration of sulfur. Subsequent degassing trends will take place from such arrays explaining the spread of data observed on the S-H_2O diagram (Fig. 7). Direct degassing from IP (Tr1), without sulfide separation, may also occur and appears as an upper limit of the former process. Finally, the IP may experience joint crystallization and degassing (Tr6) and consequent CO_2-fluxing of upward magma parcels, leading to enrichment of highly soluble sulfur and water components.

Consistent with such an early degassing, also probed on the basis of sulfur isotopes (Marini et al., 2011), the IP itself can represent an apparent initial condition, being affected by volatile infiltration (CO_2-addition) from a deeper, unsampled, exsolving primitive magma likely characterized by a lower CO_2^{TOT}/H_2O^{TOT} than the IP. This possibility is enlightened by our simulations of how CO_2-fluxing can determine a negative shift in chlorine dissolution from the 122 BC to the K-enriched MIs from recent eruptive products (Fig. 8). Such a shift of Cl^{TOT} and Cl degassing patterns is associated to a change of the Na/K ratio that may reflect vapor transport of alkalis, particularly K (e.g. Lanzafame and Ferlito, 2010; Moretti et al., 2013a). Extraction of metal cations seems in fact to increase with increasing Cl content of the gas/fluid phase (Webster et al., 2011 and references therein). Therefore, the occurrence of fluxing may partly explain the so-called

ACCEPTED MANUSCRIPT

low-K and high-K differentiation trends of Etnean magmas, as their concomitant occurrence in same products likely reflects self-mixing within degassed and undegassed, or even fluxed, parcels of the same plumbing system. This phenomenon is likely to sum up to the contribution from slab-derived fluids, which appears to be dominat in light of the inferred decoupling between alkalis and Cl (Corsaro and Métrich, 2016).

However, we cannot push further these arguments, also due to the intrinsic limits of the reported C-H-O-S-Cl-melt modeling. In fact, model results on the effects of CO_2-fluxing (Fig. 8) are based on the gas-melt chlorine partition coefficient given in Alletti et al. (2009), for which on one side the authors suggest an expression only dependent on pressure, but on the other side they report that the introduction of CO_2 in the system tends to diminish the partition coefficient. At present the latter evidences cannot lead to a H_2O/CO_2-dependent partition coefficient of Cl, in light of the uncertainty of data, which are derived by mass balance and do not allow a full characterization of the speciation state of the gaseous phase (Alletti et al., 2009). A definite assessment of the relative roles of H_2O and CO_2 on Cl dissolution requires new experimental data as well as a solubility model for chlorine accounting for chemical interactions with the other melt and gas species.

5.2 Relations with eruptive styles

By considering the ensemble of data and simulations reported in Figures 6-8, the following observations and deductions emerge:

1) An early degassing stage characterizes the deepest and least differentiated magma that is potentially common to all studied products. Such a magma is identified from MIs involved in February 1999 and 2001 activities (Fig. 6c), for which the early degassing stage coupled to deep crystallization is recognized around the IP (Tr6 in Figure 7), also according to the S-isotope modeling of Marini et al. (2011). Such an early degassing stage may produce H_2O and S-enrichment and, in particular, produces the huge flux of

ACCEPTED MANUSCRIPT

CO_2 infiltrating upward and characterizing the Etna activity (Allard et al., 1991). The early degassing stage is inferred to be a stable and major feature of the Etnean plumbing system, associated with the growth of the deep crystal mush (Allard, 1997). An early degassing stage, and consequent CO_2-fluxing, is then inferred to produce in time the switch from the 122 BC primitive magma to that involved in the recent activity (Fig. 8). Alkali transport in the fluxing gas phase may explain differences in the Na/K ratio (Fig 4), which is lower for the 122 BC and higher for products from recent activities.

2) All products record evidences of CO_2-fluxing, especially at $P \leq 100$ MPa, as shown by the TV lines (Fig. 6c,d). The upper limit of CO2-fluxing is given by the gas-buffered trend at $CO_{2(gas)}/H_2O_{(gas)} \approx 5$, which takes place for $P < 200$ MPa (Fig. 6a) and is associated with low-density and buoyant magma batches within the plumbing system.

3) Recent eruptive products show that CO_2-fluxing also characterizes deep reservoirs (P up to 200 MPa and even more), as revealed by the shift of the IP in the H_2O-S covariation of figure 7, and the position of TV lines of 1999 and 2001 products, which tend to identify more than one stocking zone of CO_2-rich volatiles (Fig. 6c). The same cannot be inferred for the 122 BC system: TV lines show the occurrence of open system conditions (Fig. 6d), suggesting the absence of important stocking volumes of volatiles within the plumbing system and prior to erupt. Furthermore, 122 BC TV lines point to H_2O-fluxing superimposing to an earlier event of CO_2-fluxing.

4) Simulations of chlorine dissolution (Fig. 8) reveal that 122 BC plinian products experience a final stage in closed-system degassing conditions, thus retaining the whole gas phase. Therefore, despite CO_2-fluxing took place throughout the 122 BC plumbing system, gas stocking and accumulation characterizes only the very late and low-P pre-eruptive stage. On the other hand, recent products are better explained by a final evolution under open-system degassing conditions, which also characterizes latest pre-eruptive conditions.

ACCEPTED MANUSCRIPT

Summarizing, CO_2-fluxing is a common phenomenon at Mt. Etna, likely related to important CO_2 release during the early stages of degassing and crystallization in the roots of the plumbing system. Nevertheless, in case of 122 BC, the continuous structure of the infiltrating flow allowed open-system degassing conditions to take place throughout the entire magmatic system, with the gas accumulating uniquely at the top of the system prior to eruption (figs. 8 and 9). This favored the subsequent H_2O-fluxing, associated to important water exsolution in the shallow system, very likely in response to crystallization. On the contrary, the plumbing system of recent activities is characterized by multiple storage levels, where the gas exsolved at large depth accumulates in magma batches evolving under closed-system conditions (Figure 9). These magma batches are well represented by products emitted in low to intermediate explosive eruptions, such as the BN 1997-98 and February 1999 episodes (Fig. 6b, 7): they rise under volatile rich conditions and experience open-system degassing conditions prior to eruption (Figs. 8 and 9). Even among the products from recent activities distinctions are possible. In fact, MIs from products relative to the February 1999 event, characterized by highly explosive phases, suggest that the erupted magma experienced lower CO_2-fluxing and dehydration compared to the BN1997-98 eruption: the Tr1 trend, representing the closed system degassing trend generated from the initial IP condition, crosses many February 1999 data, which are not particularly affected by CO_2-infiltration and which also do not represent remobilized crystals that experienced different ascent and degassing pathways (Figure 7).

We then suggest that CO_2-fluxing, hence dehydration, may be inversely related to explosivity, because produces relatively small magma batches characterized by high gas/melt ratios (up to ~ 0.3 in mass; Fig. 6a) which are mobilized upward in gas-dominated conditions. Such magma batches, being already dehydrated by CO_2-fluxing, during late decompression and pre-eruptive stages cannot exsolve high water amounts that significantly increase the explosive power: CO_2-fluxing keeps the magma supersaturated under high gas/melt ratios and inhibits the role of decompression, thus favoring the buoyancy of water-depleted small magma batches, erupted in effusive or mildly-explosive conditions. Such low-density and buoyant magma batches fall on a gas-buffered trend at

ACCEPTED MANUSCRIPT

$CO_{2(gas)}/H_2O_{(gas)} \approx 5$, a value which appears to be typical for all volcanic systems in the western Mediterranean region (Mangiacapra et al., 2008; Arienzo et al., 2010; Pino et al., 2011; Moretti et al., 2013) and which likely marks the density and rheological thresholds for buoyancy.

On the other side, data on the 122 BC pre-eruptive volatile content, along with micro-textural evidence (Sable et al. 2006), indicate that basaltic Plinian volcanism at Mt Etna in 122 BC was enabled by degassing associated with phenomena of H_2O-fluxing and high rates of bubble nucleation, decompression and magma ascent, enhanced by abundant microlite crystallization and consequent increase of magma effective viscosity (Sable et al. 2006). Such a decompression and consequent magma ascent could have been triggered by the initial emission of the volatile-rich magma evolved in closed-system degassing conditions on top of the system.

In general, we tentatively propose that explosivity at Mt. Etna may be governed by a balance involving either CO_2-fluxing (recent products) or H_2O-fluxing (122 BC) and crystallization throughout the plumbing system. If magma batches remain hydrous, also because of H_2O-fluxing, the huge and rapid exsolution of water makes them prone to erupt explosively: considering the molar weights of water and anhydrous melt, rapid exsolution of ~ 3 wt% in the last 100 MPa of decompression (Figure 6a) corresponds to the transfer of ~ 10 mol% of H_2O from the liquid to the gas phase. Fast decompression can effectively determine high H_2O super-saturation in the melt, and trigger very rapid nucleation of H_2O-dominated bubbles, leading to a strong acceleration of the magma.

We suggest, on these grounds, that it is possible to build up a criterion to understand the evolution toward either low- to mildly explosive or highly explosive –up to Plinian- eruptions at basaltic volcanoes. An important step in the application of this criterion would be the joint monitoring of ratios involving CO_2, sulfur and chlorine, in discharged gases and MIs from emitted scorias and lavas. In fact, the different roles of CO_2-fluxing and CO_2-separation could be evaluated by their contrasting effect on the solubility of other volatiles such as sulfur and halogens. For example, CO_2 addition to the system and consequent melt dehydration are expected to keep

ACCEPTED MANUSCRIPT

dissolved S as high as the IP region, until shallow degassing takes place (Figure 7). At same time, CO_2 addition and dehydration soon depress Cl dissolution in the melt (Figure 8). On the other hand, products of highly-explosive to Plinian activity should be characterized by decreasing amounts of dissolved S, probably due to early sulfide separation, but also by high contents of dissolved Cl. However, further studies on sulfur and particularly chlorine dissolution in presence of variable amounts of CO_2 are needed to confirm this internal mechanism.

5.3 Are Etnean MIs really representative of the melt-volatile equilibrium ?

By simulating melt-plagioclase equilibrium constrained by plagioclase occurrence in the alkaline lavas of Mt. Etna, Ferlito et al. (2014) and Giacomoni et al. (2015) suggest that the "high" water content found in MIs is not representative of the deep magma source, but results from H_2O-fluxing, i.e, from a process of upward water migration that would enrich the originally water-undersaturated (≤ 1.4wt%) magma ponding at various levels within the feeding system (Ferlito et al., 2014). Water fluxing within the mushy plumbing system is consistent with the late degassing of the residual gas phase formed by a continuously crystallizing magma which has already exsolved CO_2 in its early fractionation stages. However, from MIs of recent Etna products we do not have direct evidences of such a process: the possible fluxing paths that we identified involve increasing CO_2^{TOT}/H_2O^{TOT} with decreasing pressure (i.e., CO_2-fluxing), rather than a decreasing ratio as required by H_2O-fluxing (Fig. 6c). We also remark that Giacomoni et al. (2015) report results based on MELTS simulations in which CO_2 cannot be considered, such that the modeled system is necessarily underaturated at depths of interest. The role of a CO_2-rich gas phase in such simulations, together with a better appraisal of the role of fO_2, should be better investigated by experimental petrology in order to appropriately recognize the extent to which MI-based and melt-plagiocase geothermobarometries agree. For example, experimental phase equilibria on the volatile-rich K-basaltic magmas of Stromboli (Di Carlo et al., 2006), which can be considered analogous to the Etnean magma for its total volatiles ($H_2O^{TOT} \geq 3.4$ wt%, $CO_2^{TOT} \geq 2$ wt%; Aiuppa et al., 2010; Pino

ACCEPTED MANUSCRIPT

et al., 2011), shows that plagioclase crystallization, for T ≤ 1100°C and 400 MPa, occurs under hydrous conditions (dissolved H_2O ≥ 2.5 wt%). Furthermore, dissolved H_2O-CO_2 pairs from phase equilibria investigations agree with dissolved MI contents (Pichavant et al., 2009 and references therein), with H_2O^{TOT}-CO_2^{TOT} contents in the experimental charges close to those inferred from MIs. Such evidence corroborates the validity of information about volatile contents that can be extracted by MIs, at least those from the very volatile-rich active volcanoes of Southern Italy. The consistency of our water determinations, as well those of Spilliaert et al. (2006) with available independent petrologic hygrometers over the same pressure range (Armienti et al., 2013; Mollo et al., 2015) further supports our determinations.

On the contrary, 122 BC melt inclusion suggest the entrapment of a H_2O-fluxed magma at shallow depth (P ≤ 150 MPa). Therefore, it is possible that the resulting H_2O-enrichment of magma may result in the subsequent onset of diffusive phenomena throughout olivines and secondary water enrichment of hosted MIs (Hartley et al., 2015). However, we have no means to discriminate between the primary process (water fluxing itself) and the secondary one (post-entrapment diffusive H_2O gain), anyway associated to water fluxing. Diffusive H_2O-enrichment is likely to play a role in 122BC samples, subordinate to the occurrence of H_2O-fluxing. On the other hand, we can safely discount such a process for recent products as the same samples cannot simultaneously experience and provide evidence of both CO_2- and H_2O-fluxing.

Another argument against MIs representativeness involves post-entrapment disequilibrium processes (e.g., H-loss), which may offer an explanation alternative to ours to explain the observed spread of datapoints on H_2O-CO_2, H_2O-S and H_2O-Cl diagrams (Figures 6-8). For example, post-entrapment diffusive phenomena occurring in olivines may cause a fast and preferential loss of H_2O (Danyushevsky et al. 2002; Gaetani et al. 2011), which then would particularly affect the low-H_2O, high-CO_2 and high-S BN 97-98 MIs. Despite these phenomena can contribute to the dispersion displayed by the data (Figs. 3, 4, 6a, 7), they are not expected to cause dissolved H_2O to span ~3 wt%. Moreover, water loss due to post-entrapment diffusion would not question about the validity

ACCEPTED MANUSCRIPT

of H_2O-rich MIs, but of H_2O-poor MIs. Post-entrapment phenomena would then be antithetic to the above mentioned results from melt-plagioclase equilibrium modeling, which instead criticize the representativeness of high-H_2O MIs. In addition, if due to post-entrapment phenomena, the attainment of the buoyancy threshold at $CO_{2(g)}/H_2O_{(g)} \approx 5$ (Fig. 6a) would then be a fortuity, rather than the consequence of addition of CO_2 and dehydration, involving all active volcanic systems of the western Mediterranean region.

On another side, recent studies have shown that CO_2 may be transferred from the melt or glass to a coexisting vapor bubble within the MI (e.g., Esposito et al. 2011), during post-entrapment crystallization (Steele-MacInnis et al. 2011) or differential thermal contraction (Moore et al. 2015 and references therein). First of all, CO_2 corrections to measured values are not necessary as PEC can be neglected (see **Appendix**). Second, it is not disputed that in a CO_2-rich (fluxed) system such as Etna most of CO_2 must be stored into primary bubbles associated with the magma trapped as MIs. Further loss to bubble is however possible during post-entrapment cooling and contraction. This would contribute to the observed dispersion and of course to underestimating pressure (Moore et al., 2015; Wallace et al., 2015; MacIennan, 2017). However, following Wallace et al. (2015), the generally high amounts of water in our inclusions are expected to decrease the CO_2-loss to vapor bubble due to shrinkage. However, even if our recomputed pressures were underestimated, this would not diminish appreciably the representativeness of investigated MIs and our reconstruction of the Etna system. In fact the CO_2-fluxing phenomenon here recognized would be even larger, then reinforcing our findings as an explanation to the well known gas/melt imbalance of Etna, which results in too much gas compared to produced magma (e.g., Aiuppa et al., 2007). Noteworthy, our pressure estimates agree with the independent petrologic geobarometer of Armienti et al. (2013).

6. Conclusions

The trigger processes of basaltic Plinian eruptions, observed at Etna and likely many other open-vent volcanoes, are still far from being completely understood (e.g., Houghton and

ACCEPTED MANUSCRIPT

Gonnermann 2008). However, explosive basaltic volcanoes such as Etna are characterized by very abundant volatiles in the system, as testified by the contrast between the huge gas but low magma emission. How such gases are released can thus be related to the ample spectrum of activity at this volcano. In this study we have then showed that a careful analysis and modeling of degassing patterns within the H_2O-CO_2-S-Cl-melt system can give insights into the shift from low-explosive to Plinian activity. MIs in fact record the variable distribution of the amount of gas at equilibrium with melts throughout the Etna plumbing system and allow discriminating the various processes which affect its activity. These are:

1) self-mixing processes superimposing to the normal trend of fractional crystallization;
2) early degassing and crystallization of a deep (P > 200 MPa) magma, contributing to the endogenous growth of the mushy system, and releasing a huge amount of CO_2 fluxing the upward system
3) CO_2-infiltration throughout the plumbing system, which can either result in the pre-eruptive accumulation of gas at various levels within the plumbing system (recent activities), or in a direct stocking at the top of system (122 BC).
4) Subsequent H_2O-fluxing, which can be inferred for 122 BC, due to large water exsolution in the shallow magmatic system.

Gas accumulation at various levels yield high gas-melt (up to ~ 0.3 in mass, with molar $CO_{2,gas}/H_{2Ogas} \approx 5$) magma batches, which experience strong dehydration and crystallization, and which are mobilized upward in low-explosive eruption characterized by little magma emission (e.g., BN 1997-98 activity). When the huge amount of fluxing gas accumulates essentially at the top of the system, MIs show open-system degassing conditions throughout the plumbing system associated with H_2O-fluxing, but highlight the occurrence of a last pre-eruptive step in closed-system degassing conditions, likely favoured by abundant microlite crystallization and consequent increase of magma effective viscosity. This determines the Plinian activity, like in the 122 BC case. Continuous geochemical and petrologic monitoring within the H_2O-CO_2-S-Cl-melt system can thus

ACCEPTED MANUSCRIPT

help recognizing whether the magmatic system is tending to this latter scenario or not. However, further experimental studies about S and Cl dissolution at different $H_2O_{(gas)}/CO_{2(gas)}$ and gas/melt are required to attain a highly reliable parameterization.

Acknowledgements - All acquired data are given as supplementary material. Funding by PRIN-MIUR 2009 is acknowledged. The paper greatly benefited of the detailed and highly constructive review by Margaret Hartley (Univ. Manchester).

References

Aiuppa, A. (2009) Degassing of halogens from basaltic volcanism: Insights from volcanic gas observations, Chemical Geology 263, 99-109.

Aiuppa, A., Inguaggiato, S., McGonigle, A.J.S., O'Dwyer, M., Oppenheimer, C., Padgett, M.J., Rouwet, D. and Valenz,a M. (2005) H_2S fluxes from Mt. Etna, Stromboli and Vulcano (Italy) and implications for the global volcanic sulfur budget. Geochimica et Cosmochimica Acta 69-7, 1861–1871.

Aiuppa, A., Federico, C., Giudice, G., Gurrieri, S., Liuzzo, M., Shinohara, H., Favara, R. and Valenza, M. (2006) Rates of carbon dioxide plume degassing from Mount Etna volcano. Journal of Geophysical Research 111, doi: 10.1029/2006JB004307.

Aiuppa, A., Moretti, R., Federico, C., Giudice, G., Gurrieri, S., Liuzzo, M., Papale, P., Shinohara, H. and Valenza, M. (2007) Forecasting Etna eruptions by real-time observation of volcanic gas composition. Geology 35, 1115–1118.

Aiuppa, A,. Shinohara, H., Tamburello, G., Giudice, G., Liuzzo, M. and Moretti, R. (2011) Hydrogen in the gas plume of an open-vent volcano, Mount Etna, Italy. Journal of Geophysical Research 116, 1-7.

ACCEPTED MANUSCRIPT

Allard, P. (1986) Géochimique isotopique et origine de l'eau, du carbone et du soufre dans le gaz volcanique: zones de rift, marges continentales et arcs insulaires. Ph. D. thesis, Univ. Paris VII., 310 pp.

Allard, P. (1997) Endogenous magma degassing and storage at Mount Etna, Geophys. Res. Lett., 24, 2219-2221.

Allard, P., Carbonnelle, J., Dajlevic, D., Le Bronec, J., Morel P., Robe, M.C., Maurenas, J.M., Faivre-Pierret, R., Martin, D., Sabroux, J.C. and Zettwoog, P. (1991) Eruptive and diffuse emissions of CO_2 from Mount Etna. Nature 351, 387-391.

Allard, P., Behncke, B., D'Amico, S., Neri, M. and Gambino, S. (2006a) Mount Etna 1993–2005: Anatomy of an evolving eruptive cycle. Earth-Science Reviews 78, 85–114.

Allard, P., Métrich, N., Deloule, E., Belhadj, O., Mandeville,C., and Spilliaert, N. (2006b) First Ion Microprobe Determination of water and sulfur isotopic ratios in melt inclusions of olivines at Mount Etna._Eos Transactions American Geophysical Union 87, 52, Fall Meeting Supplement, Abstract V13D-08.

Alletti, M., Baker, D.R., Scaillet, B., Aiuppa, A., Moretti, R. and Ottolini, L. (2009) Chlorine partitioning between a basaltic melt and H_2O-CO_2 fluids at Mount Etna. Chemical Geology 263, 37-50.

Arienzo I, Moretti R, Civetta L, Orsi G. and Papale P (2010) The feeding system of Agnano–Monte Spina eruption (Campi Flegrei, Italy): Dragging the past into present activity and future scenarios. Chem Geol 270, 135–147.

Armienti, P., Tonarin,i S., D'Orazio, M. and Innocenti, F. (2004) Genesis and Evolution of Mt Etna alkaline lavas: petrological and Sr-Nd-B isotope constraints. Periodico di Mineralogia 73, 29-52.

Armienti, P., Perinelli, C., and Putirka, K. D. (2013). A new model to estimate deep-level magma ascent rates, with applications to Mt. Etna (Sicily, Italy). Journal of Petrology, 54, 795-813.

ACCEPTED MANUSCRIPT

Barsanti, M., Papale, P., Barbato, D., Moretti, R., Hauri, E., Boschi, E. and Longo, A. (2009) Heterogeneous large total CO_2 abundance in the shallow magmatic system of Kilauea volcano Hawaii. Journal of Geophysical Research 114, B12201.

Blank, J. G. and Brooker, R. A. (1994) Experimental studies of carbon dioxide in silicate melts: solubility, speciation and stable isotope behavior. In Volatiles in Magmas (ed. M.R. Carroll & J.R. Hollo-way) MSA Rev. Mineral. 30,157–186

Blundy, J., and Cashman, K. (2008) Petrologic reconstruction of magmatic system variables and processes. Reviews in Mineralogy and Geochemistry, 69, 179-239.

Bonnin-Mosbah, M., Simionovici, A. S., Métrich, N., Duraud, J. P., Massare, D., and Dillmann, P. (2001). Iron oxidation states in silicate glass fragments and glass inclusions with a XANES micro-probe. Journal of Non-Crystalline Solids, 288, 103-113.

Burgisser, A. and Scaillet, B. (2007) Redox evolution of a degassing magma rising to the surface. Nature 445, 194-197.

Burton, M., Murè, F., Allard, P. and Oppenheimer, C. (2004) FTIR remote sensing of fractional magma degassing at Mount Etna, Sicily. Geological Society Special Publication 213 , 281-293

Chiodini, G., Caliro, S., Aiuppa, A., Avino, R., Granieri, D., Moretti, R. and Parello, F. (2011) First $^{13}C/^{12}C$ isotopic characterisation of volcanic plume CO_2. Bulletin of Volcanology 73, 531-542.

Clocchiatti, R., Weisz, J., Mosbah, M. and Tanguy, J.C. (1992) - Coexistence de «verres» alcalins et tholeiiliques saturés en CO_2 dans les olivines des hyaloclastites d'Aci Castello (Etna Sicile, Italie). Arguments en faveur d'un manteau anormal et d'un reservoir profond. Acta Vulcanologica 2, 16 1- 173.

Collins, S.J., Pyle, D.M. and Maclennan, J. (2009) Melt inclusions track pre-eruption storage and dehydration of magmas at Etna. Geology 37, 571-574.

Collins, S.J., Maclennan, J., Pyle, D.M., Barnes, S.J. and Upton, B.G.J. (2012) Two phases of sulphide saturation in Reunion magmas: Evidence from cumulates. Earth and Planetary Science Letters 337–338 , 104–113.

ACCEPTED MANUSCRIPT

Coltelli, M., Del Carlo, P. and Vezzoli, L. (1998) Discovery of a Plinian basaltic eruption of Roman age at Etna volcano, Italy. Geology 12, 1095-1098.

Coltelli, M., Del Carlo, P. and Vezzoli, L. (2000) Stratigraphic constraints for explosive activity in the last 100 ka at Etna volcano, Italy. International Journal of Earth Sciences 89, 665–677.

Condomines, M., Tanguy, J.C., Kieffer, G. and Allègre, C.J. (1982) Magma evolution of a volcano studied by 230Th-238U disequilibrium and trace element systematics: the Etna case. Geochimica et Cosmochimica Acta 46, 1397–1416.

Condomines, M., Tanguy, J.C. and Michaud, V. (1995) Magma dynamics at Mt Etna : constraints from U–Th–Ra–Pb radioactive disequilibria and Sr isotopes in historical lavas. Earth and Planetary Science Letters 132, 25–41.

Corsaro, R.A., Métrich, N., Allard,. P., Andronico, D., Miraglia, L. and Fourmentraux, C. (2009) The 1974 flank eruption of Mount Etna: An archetype for deep dike-fed eruptions at basaltic volcanoes and a milestone in Etna's recent history. Journal of Geophysical Research 114, B07204.

Corsaro, R.A., Di Renzo, V., Distefano, S., Miraglia, L. and Civetta, L. (2013) Relationship between magmatic processes in the plumbing system of Mt. Etna and the dynamics of the eastern flank: inferences from the petrologic study of the products erupted from 1995 to 2005. Journal of Volcanology and Geothermal Research 251, 75-89.

Corsaro, R. A., and Métrich, N. (2016). Chemical heterogeneity of Mt. Etna magmas in the last 15ka. Inferences on their mantle sources. Lithos, 252, 123-134.

Danyushevsky, L. V., Della-Pasqua, F. N., and Sokolov, S. (2000). Re-equilibration of melt inclusions trapped by magnesian olivine phenocrysts from subduction-related magmas: petrological implications. Contributions to Mineralogy and Petrology, 138, 68-83.

Del Carlo, P. and Pompilio, M. (2004) The relationship between volatile content and the eruptive style of basaltic magma: The Etna case. Annals of Geophysics 47, 1423– 1432.

ACCEPTED MANUSCRIPT

Di Carlo, I., Pichavant, M., Rotolo, S. G., and Scaillet, B. (2006). Experimental crystallization of a high-K arc basalt: the golden pumice, Stromboli volcano (Italy). Journal of Petrology, 47(7), 1317-1343.

Dixon, J.E., Stolper, E.M. and Holloway, J.R. (1995) An experimental study of water and carbon dioxide solubilities in mid-ocean ridge basaltic liquids. part I: Calibration and solubility models. Journal of Petrology 36, 1607-1631.

Doglioni, C., Harabaglia, P., Martinelli, G., Mongelli, F. and Zito, G. (1996) A geodynamic model of the southern Apennines accretionary prism. Terra Nova 8, 540 – 547.

Esposito, R., Bodnar, R. J., Danyushevsky, L. V., De Vivo, B., Fedele, L., Hunter, J., lima, A., and Shimizu, N. (2011). Volatile evolution of magma associated with the Solchiaro eruption in the Phlegrean Volcanic District (Italy). Journal of Petrology, 52, 2431-2460.

Ferlito, C., Viccaro, M. and Cristofolini, R. (2008) Volatile induced differentiation in the plumbing system of Mt. Etna volcano (Italy): evidence from glass tephra of the 2001 eruption. Bulletin of Volcanology 70, 4, 455–473.

Ferlito, C. and Lanzafame, G. (2010) The role of supercritical fluids in the potassium enrichment of magmas at Mount Etna volcano (Italy). Lithos 119-3, 642-650.

Ferlito, C., Coltorti, M., Lanzafame, G., and Giacomoni, P. P. (2014). The volatile flushing triggers eruptions at open conduit volcanoes: Evidence from Mount Etna volcano (Italy). Lithos, 184, 447-455.

Fine, G., & Stolper, E. (1986). Dissolved carbon dioxide in basaltic glasses: concentrations and speciation. Earth and Planetary Science Letters, 76(3-4), 263-278.Gaetani, G., O'Leary, J. and Shimizu, N. (2011). Post-entrapment changes to H_2O and CO_2 in olivine-hosted melt inclusions. Goldschmidt 2011 Conference Abstracts, Mineralogical Magazine 75, 879.

Gerlach, T.M. (1979) Evaluation and restoration of the 1970 volcanic gas analyses from Mount Etna, Sicily. Journal of Volcanology and Geothermal Research 6, 165-178.

ACCEPTED MANUSCRIPT

Giacomoni, P. P., Ferlito, C., Coltorti, M., Bonadiman, C., and Lanzafame, G. (2014). Plagioclase as archive of magma ascent dynamics on “open conduit” volcanoes: The 2001–2006 eruptive period at Mt. Etna. Earth-Science Reviews, 138, 371-393.

Giammanco, S., Inguaggiato, S. and Valenza, M. (1998) Soil and fumarole gases of Mount Etna: geochemistry and relations with volcanic activity. Journal of Volcanology and Geothermal Research 81, 297-310.

Gillot, P.Y., Kieffer, G. and Romano, R. (1994) The evolution of Mount Etna in the light of potassium-argon dating. Acta Vulcanologica 5, 81–87.

Hartley, M. E., Neave, D. A., Maclennan, J., Edmonds, M., and Thordarson, T. (2015). Diffusive over-hydration of olivine-hosted melt inclusions. Earth and Planetary Science Letters, 425, 168-178.

Holloway, J. R. and Blank, J. G. (1994) Application of experimental results to C-O-H species in natural melts. In Reviews in Mineralogy (Ed. P. H. Ribbe). Mineralogical Society of America.

Houghton, B.F. and Gonnermann, H.M. (2008) Basaltic explosive volcanism: Constraints from deposits and models. Chemie der Erde – Geochemistry 68, 117-140.

Huntingdon, A.T. (1973) The collection and analysis of volcanic gases from Mount Etna. Philosophical transactions of the Royal Society of London Series A 274, 119-128.

Kamenetsky, V.S., Pompilio, M., Métrich, N., Sobolev, A.V., Kuzmin, D.V. and Thomas, R. (2007) Arrival of extremely volatile-rich high-Mg magmas changes explosivity of Mount Etna. Geology 35, 255-258.

Kahl, M., Chakraborty, S., Pompilio, M., and Costa, F. (2015). Constraints on the nature and evolution of the magma plumbing system of Mt. Etna volcano (1991–2008) from a combined thermodynamic and kinetic modelling of the compositional record of minerals. Journal of Petrology, 56(10), 2025-2068.

Kieffer, G. (1985) Évolution structrurale et dynamique d'un grand volcan polygénique: stades d'édification et activité actuelle de l'Etna. Ph. D. thesis, Univ. de Clermont Ferrand II.

ACCEPTED MANUSCRIPT

ACCEPTED MANUSCRIPT

Kieffer, G. and Tanguy, J.C. (1993) L'Etna: évolution structurale, magmatique et dynamique d'un volcan "polygénique". Mémoires de la Société Géologique de France 163, 253-271.

La Delfa, S., Patanè, G., Clocchiatti, R., Joron, J.L. and Tanguy, J.C. (2001) Activity of Mount Etna preceding the February 1999 fissure eruption: inferred mechanism from seismological and geochemical data. Journal of Volcanology and Geothermal Research 105, 121–139.

Lange, R. A. (1994) The effect of H_2O, CO_2 and F on the density and viscosity of silicate melts. In *Volatiles in Magmas* (eds. M. R. Carroll and J. R. Holloway), pp. 331–369. Reviews in Mineralogy 30, Mineralogical Society of America.

Le Guern, F. (1988) Ecoulements gazeux réactifs à hautes températures, mesures et modélisation. Ph. D. thesis, Paris Univ.

Le Maitre, R.W. (1989) A Classification of Igneous Rocks and Glossary of Terms. Recommendations of the IUGS Subcommission of Systematic of Igneous rocks. Blackwell Scientific, London.

Lentini, F. (1982) The geology of the Mt. Etna basement. Memorie della Società Geologica Italiana 23, 7–25.

Lesne, P., Kohn, S. C., Blundy, J., Witham, F., Botcharnikov, R. E., and Behrens, H. (2011). Experimental simulation of closed-system degassing in the system basalt–H_2O–CO_2–S–Cl. Journal of Petrology, 52, 1737-1762.

Maclennan, J. (2017). Bubble formation and decrepitation control the CO_2 content of olivine- hosted melt inclusions. Geochemistry, Geophysics, Geosystems, 18, 597-616.

Mangiacapra, A., Moretti, R., Rutherford, M., Civetta, L., Orsi, G., and Papale, P. (2008). The deep magmatic system of the Campi Flegrei caldera (Italy). Geophysical Research Letters, 35(21).

Marianelli, P., Métrich, N., and Sbrana, A. (1999). Shallow and deep reservoirs involved in magma supply of the 1944 eruption of Vesuvius. Bulletin of Volcanology, 61(1-2), 48-63.

Marini, L., Moretti, R. and Accornero, M. (2011) Sulfur Isotopes in Magmatic-Hydrothermal Systems, Melts, and Magmas. Reviews in Mineralogy and Geochemistry 73, 423-492.

ACCEPTED MANUSCRIPT

Métrich, N. and Wallace, P. (2011) Volatile Abundances in Basaltic Magmas and Their Degassing Paths Tracked by Melt Inclusions. Reviews in Mineralogy and Geochemistry 69, 363-402.

Metrich, N., Clocchiatti, R., Mosbah, M. and Chaussidon, M (1993) The 1989-1990 activity of Etna: magma mingling and ascent of H_2O-Cl-S-rich basaltic magma - evidence from melt inclusions. Jounnal of Volcanology and Geothermal Research 59, 131-144.

Métrich, N., Bertagnini,A., Landi, P. and Rosi, M. (2001) Crystallization Driven by Decompression and Water Loss at Stromboli Volcano (Aeolian Islands, Italy). Journal of Petrology 42-8, 1471-1490.

Métrich, N., Allard, P., Spilliaert, N., Andronico, D. and Burton, M. (2004) 2001 flank eruption of the alkali- and volatile-rich primitive basalt responsible for Mount Etna's evolution in the last three decades. Earth and Planetary Science Letters 228,1-17.

Mollo, S., Giacomoni, P. P., Coltorti, M., Ferlito, C., Iezzi, G., and Scarlato, P. (2015). Reconstruction of magmatic variables governing recent Etnean eruptions: Constraints from mineral chemistry and P–T–fO_2–H_2O modeling. Lithos, 212, 311-320.

Moore, L. R., Gazel, E., Tuohy, R., Lloyd, A. S., Esposito, R., Steele-MacInnis, M., Hauri, E., Wallace, P. J., Plank, T., and Bodnar, R. J. (2015). Bubbles matter: An assessment of the contribution of vapor bubbles to melt inclusion volatile budgets. American Mineralogist, 100(4), 806-823.

Moretti, R., and Ottonello, G. (2003). A polymeric approach to the sulfide capacity of silicate slags and melts. Metallurgical and Materials Transactions B, 34(4), 399-410.

Moretti, R., and Ottonello, G. (2003). Polymerization and disproportionation of iron and sulfur in silicate melts: insights from an optical basicity-based approach. Journal of Non-Crystalline Solids, 323(1), 111-119.

Moretti, R., and Ottonello, G. (2005). Solubility and speciation of sulfur in silicate melts: The Conjugated Toop-Samis-Flood-Grjotheim (CTSFG) model. Geochimica et Cosmochimica Acta, 69(4), 801-823.

ACCEPTED MANUSCRIPT

Moretti, R. and Papale, P. (2004) On the oxidation state and volatile behaviour in multicomponent gas-melt equilibria. Chemical Geology 213, 265–280.

Moretti, R., Papale, P. and Ottonello, G. (2003) A model for the saturation of C-H-O-S fluids in silicate melts. In Volcanic Degassing (eds. C., Oppenheimer, D.M. Pyle and J. Barclay). Geological Society of London, Special Publications 213, pp. 81–101.

Moretti R., Arienzo I., Civetta L., Orsi G. and D'Antonio M. (2013a) The deep plumbing system of the Ischia island: a physico-chemical window on the fluid-saturated and CO_2-sustained Neapolitan volcanism (Southern Italy). Journal of Petrology, 54, 951-984

Moretti R., Arienzo I., Civetta L., Orsi G. and Papale P. (2013b) Multiple magma degassing sources at an explosive volcano. Earth and Planetary Sciences Letters,367, 95-104

Murru M., Montuori C., Wyss M. and Privitera E. (1999). The locations of magma chambers at Mt. Etna, Italy, mapped by b-values. Geophysical Research Letters 26, 2553-2556.

Newman, S. and Lowenstern, J.B. (2002) VolatileCalc: a silicate melt-H2O-CO2 solution model written in Visual Basic for Excel. Computers and Geosciences 28, 597-604.

Oppenheimer, C., Moretti, R., Kyle P., Eschenbacher, A., Lowenstern, J., Hervig, R. and Dunbar, N. (2011) Mantle to surface gas trigger of the alkalic intraplate Erebus volcano, Antarctica. Earth and Planetary Science Letters 306, 261-271.

Paonita, A., A. Caracausi, G. Iacono-Marziano, M. Martelli, and A. Rizzo (2012), Geochemical evidence for mixing between fluids exsolved at different depths in the magmatic system of Mt Etna (Italy), Geochim. Cosmochim. Acta, 84, 380–394.

Papale P. (1999) Strain-induced magma fragmentation in explosive eruptions. Nature 397, 425-428.

Papale P. (2005) Determination of total H_2O and CO_2 budgets in evolving magmas from melt inclusion data. Journal of Geophysical Research 110, doi:10.1029/2004JB003033.

Papale, P., Moretti, R., and Barbato, D. (2006) The compositional dependence of the saturation surface of H_2O+CO_2 fluids in silicate melts. Chemical Geology 229,78-95.

ACCEPTED MANUSCRIPT

Peccerillo, A. (2005) Plio-Quaternary volcanism in Italy. Petrology, Geochemistry, Geodynamics. Springer, Heidelberg.

Pichavant, M., Di Carlo, I., Le Gac, Y., Rotolo, S. G., and Scaillet, B. (2009). Experimental constraints on the deep magma feeding system at Stromboli volcano, Italy. Journal of Petrology, 50(4), 601-624.

Pino, N. A., Moretti, R., Allard, P., and Boschi, E. (2011). Seismic precursors of a basaltic paroxysmal explosion track deep gas accumulation and slug upraise. Journal of Geophysical Research: Solid Earth, 116(B2).

Rizzo, A. L., Jost, H. J., Caracausi, A., Paonita, A., Liotta, M., and Martelli, M. (2014). Real- time measurements of the concentration and isotope composition of atmospheric and volcanic CO_2 at Mount Etna (Italy). Geophysical Research Letters, 41(7), 2382-2389.

Rizzo, A. L., Liuzzo, M., Ancellin, M. A., & Jost, H. J. (2015). Real-time measurements of $\delta^{13}C$, CO_2 concentration, and CO_2/SO^2 in volcanic plume gases at Mount Etna, Italy, over 5 consecutive days. Chemical Geology, 411, 182-191.

Roeder, P. L., and Emslie, R. (1970). Olivine-liquid equilibrium. Contributions to Mineralogy and Petrology, 29, 275-289.

Sable, J.E., Houghton, B.F., Del Carlo, P. and Coltelli, M. (2006) Changing conditions of magma ascent and fragmentation during the Etna 122BC basaltic Plinian eruption: evidence from clast microtextures. Journal of Volcanology and Geothermal Research 158, 333–354.

Scaillet, B. and Pichavant, M. (2005) A model of sulphur solubility for hydrous mafic melts: application to the determination of magmatic fluid compositions of Italian volcanoes. Annals Geophysics 48, 671-698.

Spilliaert, N., Allard, P., Metrich, N., and Sobolev, A.V. (2006a) Melt inclusion record of the conditions of ascent, degassing, and extrusion of volatile-rich alkali basalt during the powerful 2002 flank eruption of Mount Etna (Italy). Journal of Geophysical Research 111, doi: 10.1029/2005JB003934.

ACCEPTED MANUSCRIPT

Spilliaert, N., Metrich, N., and Allard, P. (2006b) S-Cl-F degassing pattern of water rich alkali basalt: modelling and relationship with eruption styles on Mount Etna Volcano. Earth and Planetary Science Letters 248, 772–786.

Steele-Macinnis, M., Esposito, R., and Bodnar, R. J. (2011). Thermodynamic model for the effect of post-entrapment crystallization on the H_2O–CO_2 systematics of vapor-saturated, silicate melt inclusions. Journal of Petrology, 52(12), 2461-2482.

Symonds, R.B., Rose, W.I., Bluth, G.J.S., and Gerlach, T.M. (1994) Volcanic-gas studies: methods, results, and applications. In Volatiles in magmas (eds. M.R. Carroll and J.R. Holloway). Reviews in Mineralogy 30, 1-66

Tanguy, J.C. and Kieffe,r G. (1993) Les éruptions de l'Etna et leurs mécanismes. Mémoires de la Société géologique de France 163, 239-252.

Tonarini, S., Armienti, P., D'Orazio, M., and Innocenti, F. (2001) Subduction-like fluids in the genesis of Mt. Etna magmas: evidence from boron isotopes and fluid mobile elements. Earth and Planetary Science Letters 192,471–483.

Wallace, P. J., Kamenetsky, V. S., and Cervantes, P. (2015). Melt inclusion CO2 contents, pressures of olivine crystallization, and the problem of shrinkage bubbles. American Mineralogist, 100, 787-794.

ACCEPTED MANUSCRIPT

ACCEPTED MANUSCRIPT

Figure Captions

Figure 1. Sketch of the Etna plumbing system (modified after Murru et al. 1999), showing onset of degassing since large depth (e.g., Clocchiatti et al. 1992; Kamenetsky et al. 2007) and the presence of a deep magma storage and of a cumulitic body in the 4 to 10 km depth range. White circles represents exsolved gases/fluids. Question marks account for the unknown geometry and uncertain continuity of the connection between reservoirs.

Figure 2. TAS diagram of samples object of this study. Only in this case, data (see **Supplementary Material**) were normalized to 100% on a volatile-free basis. The transparent white field reports whole rocks data (from Armienti et al., 2004). Analytical uncertainty within symbol size.

Figure 3. Concentration of dissolved H_2O (**panel a**), CO_2 (**panel b**), S (**panel c**) and Cl (**panel d**)in MIs vs. forsterite content (mol %) of their host olivines. Data correspond to original measurements reported in the **Supplementary Material**. Analytical uncertainties are 10% for H_2O, 20% for CO_2 and within symbol size for MgO and Fo content.

Figure 4. Panel a) Plots of Na_2O vs K_2O, allows discriminating among magmas characterized by low-K and high-K contents. **Panel b**) Plot of P_2O_5 vs K_2O, **Panel c)** Plot of Cl vs K_2O, **Panel d)** Plot of H_2O vs K_2O, **Panel e)** Plot of CO_2 vs K_2O, **Panel f)** Plot of S vs K_2O. Data correspond to original measurements reported in the **Supplementary Material**. Analytical uncertainty is within symbol size with the exception of H_2O (10%) and CO_2 (25%).

Figure 5. Etna MI hosted in olivines coexisting with sulfide globules and multiple oxide minerals. Note the typical association MI-oxide-sulfide globule, which has also been found in clinopyroxene

ACCEPTED MANUSCRIPT

and plagioclase crystal (not shown). Upper panel: transmission light microphotograph. Lower panel: reflected-light microphotograph.

Figure 6. Panel a): saturation isobars for dissolved H_2O and CO_2 contents in Etnean melts, based on the saturation model of Papale et al. (2006). Datapoints from the SEC February 1999, BN 1997-1998 and 122 BC MIs (the latter including H_2O-CO_2 determinations from Del Carlo and Pompilio, 2004) and fields from the literature (green contour line: Spilliaert et al. 2006a; black contour line: Kamenetsky et al. 2007) have been reported. The degassing trend bounding the ensemble of data on the right is for closed-system conditions with H_2O^{TOT} = 4 wt% and CO_2^{TOT} = 2 wt%. Analytical uncertainties are 10% for H_2O and 25% for CO_2. **Panel b)** TV lines theory (Papale 2005) is summarized for closed-system conditions. The main figure reports the case of one MI and its TV line; the panel inset shows the ideal case of dissolved H_2O-CO_2 contents in many MIs connected by a unique degassing paths: the generated many TV lines cross in one point, corresponding to the total H_2O and total CO_2 contents featuring the closed-system degassing path. **Panel c)** TV lines generated by measured H_2O-CO_2 pairs in MI samples from BN 1997-98 activity (dashed black lines), SEC February 1999 (black solid lines) and 2001 eruption (green lines) are displayed. Note that the two TV lines derived from the 2001 eruption products (solid green lines) cross at same CO_2^{TOT}, but at higher H_2O^{TOT}values (3.8 wt%) with respect to 1997-98 and 1999 samples (3.4 wt%). Also note the steepness of TV lines for dehydrated samples pertaining to BN 1997-98 activity. H_2O^{TOT} from 3.4 to 3.8 wt% and CO_2^{TOT} = 1.92 wt% define the initial set of total volatiles for magma degassing (reported as an ellipse embracing these values). TV lines cross-over points falling on the left of such circle denote fluxed conditions, yielding CO_2-enrichment and dehydration. **Panel d)** TV lines for 122 BC eruptions (solid blue lines: this study; dashed blue lines: Del Carlo and Pompilio 2004) are reported. Note the many TV lines from 122 BC yielding very low $CO2^{TOT}$ values.

ACCEPTED MANUSCRIPT

Figure 7. Panel a) Covariation of dissolved H_2O and S. Degassing trends for -3≤NNO≤3 are traced, all starting from the same initial condition of total volatile contents. Note however that the trends in figure cannot and must not start from a unique point, even though total volatiles are fixed. This generates a spread (located within the IP; gray dotted ellipse) because the changing redox conditions change sulfur solubility which affects the whole saturation surface in H_2O-CO_2-S. Analytical uncertainty within symbol size. **Panel b)** Covariation of dissolved H_2O and S. Three main degassing trends are distinguished, computed in the C-H-O-S-melt system (Moretti et al. 2003; Moretti and Papale, 2004) for NNO redox conditions. The possible variations of total volatile contents in H_2O and S were considered as a shift outside the Initial Pole region (IP; gray dotted ellipse). See text for an explanation of trends Tr1 to Tr6. **Both panels**: raw data are plotted (**Supplementary Material)**; analytical uncertainty within symbol size for S and 10% for H_2O.

Figure 8. Covariation of dissolved H_2O and Cl (raw data as in the **Supplementary Material**). Degassing trends, generated by integrating C-H-O-S-melt computations with chlorine partitioning (Alletti et al. 2009). allow inspecting the chlorine evolution by degassing, until crystallization takes place in dehydrated samples. Solid patterns: closed systems; dashed black pattern: open-system with crystallization; transversal dotted gray line: 20 MPa isobar marking the onset of appreciable crystallization while degassing (eq. 1). CO_2-fluxing can determine chlorine depression in the melt phase, allowing the system to switch from Na-rich (122 BC) to K-rich (recent products) systems. Two fluxing paths are drawn (cyan dashed line: pure CO_2; orange dashed line: CO_2/H_2O = 95/5 in mass). Analytical uncertainty within symbol size for Cl and 10% for H_2O.

Figure 9. Conceptual model (modified from Ferlito et al., 2014) summarizing pre-eruptive conditions of 122 BC (**panel a**) and recent activities (**panel b**) along with the main degassing processes within the Etnean plumbing system. Both systems experience strong CO_2-fluxing (small

ACCEPTED MANUSCRIPT

yellow ellipses) since a depth corresponding to ~400 MPa (at least). This produces a CO_2 cap on top of the 122BC system but gas dominated magma batches (large two-colours ellipses) in recent activity. In case of 122BC water fluxing (small cyan ellipses) in the shallow system overprints the previous CO-fluxing and is accompanied by diffuses crystallization (black dispersed chips). Endogenus growth (Allard, 1997) explains why the plumbing system for recent activity was pictured bigger than the 122BC one.

Appendix

A1. H_2O and CO_2 analytical determinations

H_2O and CO_2 measurements were made in transmission model, by using KBr as beam-splitter and a HgCdTe (MCT) detector. Running configuration was based on 1536 scans, a resolution of 8 cm^{-1}, a mirror speed of 1.8988 cm/s and aperture of 90. The concentrations of H_2O and carbon of inclusions is calculated through the Beer-Lambert law

$$C = \frac{A \times M}{\varepsilon \times \rho \times e} \times 100 \text{ (wt \%)} \qquad \text{(A1)}$$

where A is the measured absorbance; M is the molar weight; e is the sample thickness; ρ is the density; ε is the coefficient of molar absorption. Density was calculated stemming from the data of Lange (1994). Thickness measurements have been taken by means of a Mitutoyo™ digital comparator, which precision is about 1µm. The measurements of absorbance for H_2O has been carried on the peak at 3530 cm^{-1}. In order to avoid errors on the evaluation of both density and absorption coefficients, we correlated the measured absorbances/thickness ratios with *ad hoc* determinations made on synthetic glasses of Etnean composition. A lava sample was doped with respect to H_2O at high T and P and total H_2O concentration (up to 3.5 wt%). H_2O contents were determined through Karl Fisher titration at the Institut des Science de la Terre (ISTO) in Orléans on an etnean lava sample remelted and doped with H_2O up to 3.5 wt%. A specific calibration for

ACCEPTED MANUSCRIPT

Etnean glasses is given in Figure A1 and shows that equation A1 reduces to $C_{H_2O^{TOT}(wt\%)} \cong \frac{A_{3530}}{e} \times 100$.

Carbon is present in studied inclusions only as carbonates CO_3^{2-} (Holloway and Blank 1994; Blank and Brooker 1994). The measurement is made through the peak at 1515 cm^{-1}, whose absorption coefficient, ε_{1515}, has been determined according to Dixon et al. (1995) as a function of the atom ratio Na/(Na+Ca). Because the carbonate doublet including the peak of interest is located on the shoulder of the large absorption domain of the silicate network, absorbance was estimated only after the subtraction of the spectrum of an identical but volatile-free glass. Thus, we subtracted to each spectrum both an oxidised and a reduced spectrum of reference, thus averaging the two absorbance values obtained through peak deconvolution. FTIR-estimated errors are 10% for H_2O and at most 25% for CO_2, by considering the intervening factors as independent variables.

A2. About Post Entrapment Crystallization (PEC)

PEC determined a compositional shift tending obviously to override the original melt-crystal equilibrium. Its effect is to magnify the differences in Mg, Na, and Si abundances between MIs and glass-matrix.

Figure A2 shows that MIs evolved in response to crystallization, and that post-entrapment modifications are weak and negligible (MgO of MIs and WRs encompass the same range of variation). MI re-equilibration during magma ascent (Danyushevsky et al., 2000) is then inadequate to explain observed values in MIs, particularly the FeO and, to a large extent, MgO constancy with respect to the olivine Fo content (Figure A2a,b).

Also note that the PEC shift does not explain the variability within a single olivine grain (see **Supplementary Data**). As a matter of fact, the compositional variations of major and also volatile elements of the Etna are quite independent of the host crystal chemistry, as evidenced by appreciable chemical differences recorded by MIs within a single homogeneous crystal grain.

ACCEPTED MANUSCRIPT

We have also computed Fe^{3+}/Fe_{tot} values on the basis of Roeder and Emslie (1970), who defined a temperature independent coefficient for the Fe/Mg exchange between olivine and coexisting liquid basalt (K_D=0.3). Fe^{3+}/Fe_{tot} values range from zero up to 0.62 in one BC sample (Figure A3a). This wide range is in line with the two log units of variations in fO_2, related to water exsolution during magma ascent in the conduit and magma emplacement near the surface (Moretti and Papale, 2004; Burgisser and Scaillet, 2007; Mollo et al., 2015).

We however considered the role that PEC may have occurred and thus affected the original redox state of iron. If PEC occurred, it should have increased the Fe^{3+}/Fe_{tot} ratio because of FeO removal from the liquid. We then assumed a low Fe^{3+}/Fe_{tot} value of 0.2, which is a lowermost value in our dataset common to the whole compositional range (Figure A3a) and which corresponds to XANES measurements by Bonnin-Mosbah et al. (2001). We then back-calculated MI compositions by adding to each MI composition FeO, MgO, SiO_2 aliquots corresponding to the surrounding host olivine until the 0.2 iron redox ratio was attained. Computed values (Figure A3b) show that even under this –quite extreme- redox assumption, crystallization would be at most 7%, peaking to 11% for only one MI from the 122BC. In our exercise the larger the difference in redox state, the larger the extent of PEC, which explains why the computed PEC shows the same trend increasing with olivine Fo content as for the iron redox state from Fe/Mg olivine-liquid partitioning (Figure A3).

Given the small extent of PEC, encompassed by EMPA errors, we discard post-entrapment effects and safely use raw analytical data. Considering the focus of our study (volatile contents and their interpretation) we can state that the PEC effect does not alter at all the solubility properties of the melt and its mass balance for volatiles.

Appendix figure caption

ACCEPTED MANUSCRIPT

Figure A1. *Ad hoc* correlation for Abs_{3530}/Thickness and H_2O wt% in etnean glasses. Thickness dimension is micron. Note that the slope of the correlation line is one, also implying that $M/\varepsilon \times \rho$ in equation A1 is one.

Figure A2. Covariation diagrams for PEC assessment. **Panel a**) CaO/Al_2O_3 vs MgO for studied MIs and related whole rock. **Panel b**), FeO_{tot} vs MgO for studied MIs and related whole rocks. **Panel c**), host olivine Fo-contents vs MgO for studied MIs. **Panel d**) host olivine Fo-content vs MgO for studied MIs. **Both panels**: Data correspond to original measurements reported in the Supplementary Material. Analytical uncertainty within symbol size.

Figure A3. Redox-based PEC assessment. **Panel a**) Iron oxidation state (based on olivine/basalt FeO/MgO exchange; Roeder and Emslie, 1970) vs host olivine Fo-contents for studied MIs. Computed redox data are given in **Supplementary Material**. **Panel b**) Amount of post-entrapment crystallization required to match an iron redox ratio of 0.2 (see text for details).

ACCEPTED MANUSCRIPT

ACCEPTED MANUSCRIPT

Figure 1

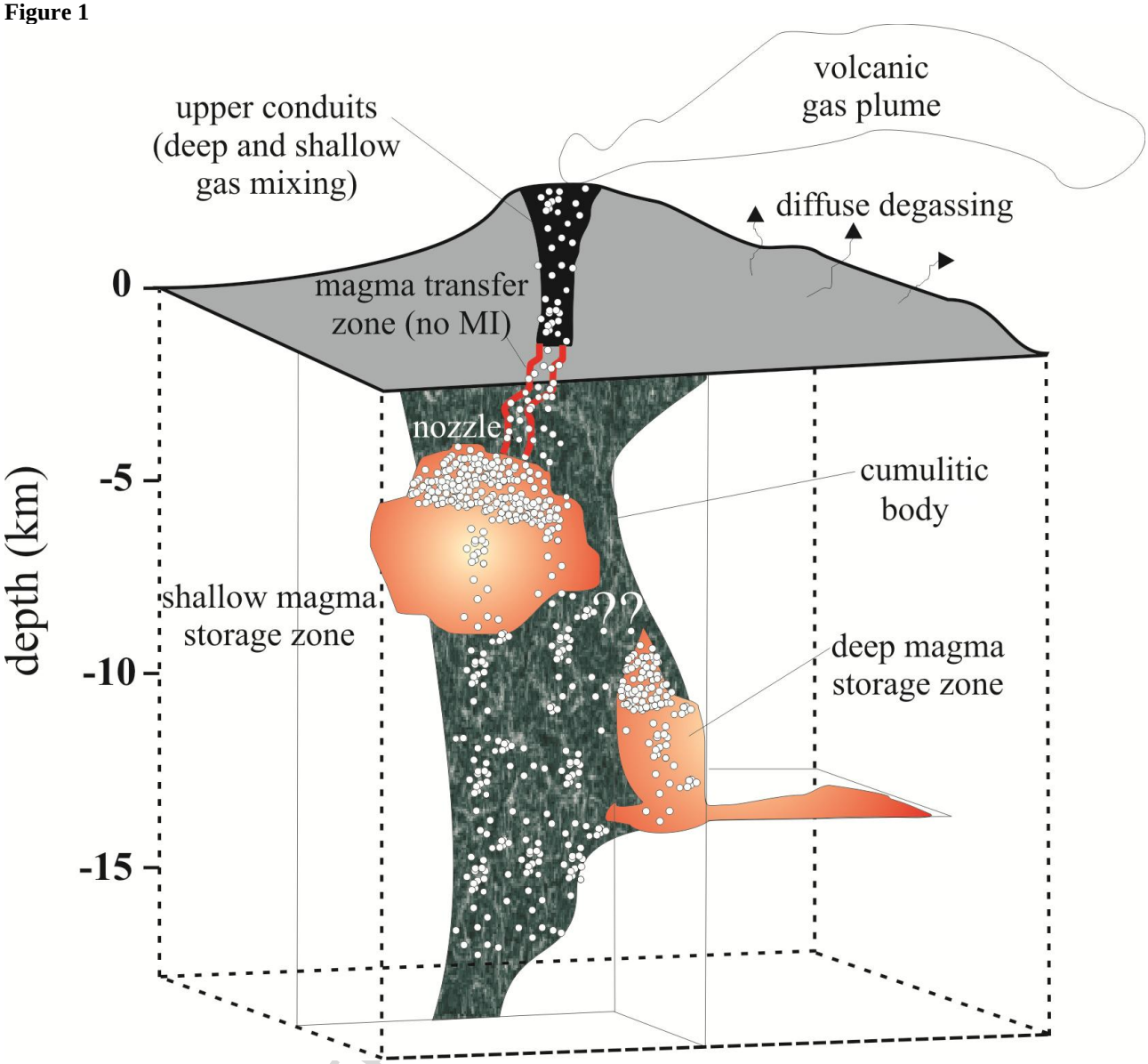

ACCEPTED

ACCEPTED MANUSCRIPT

Figure 2

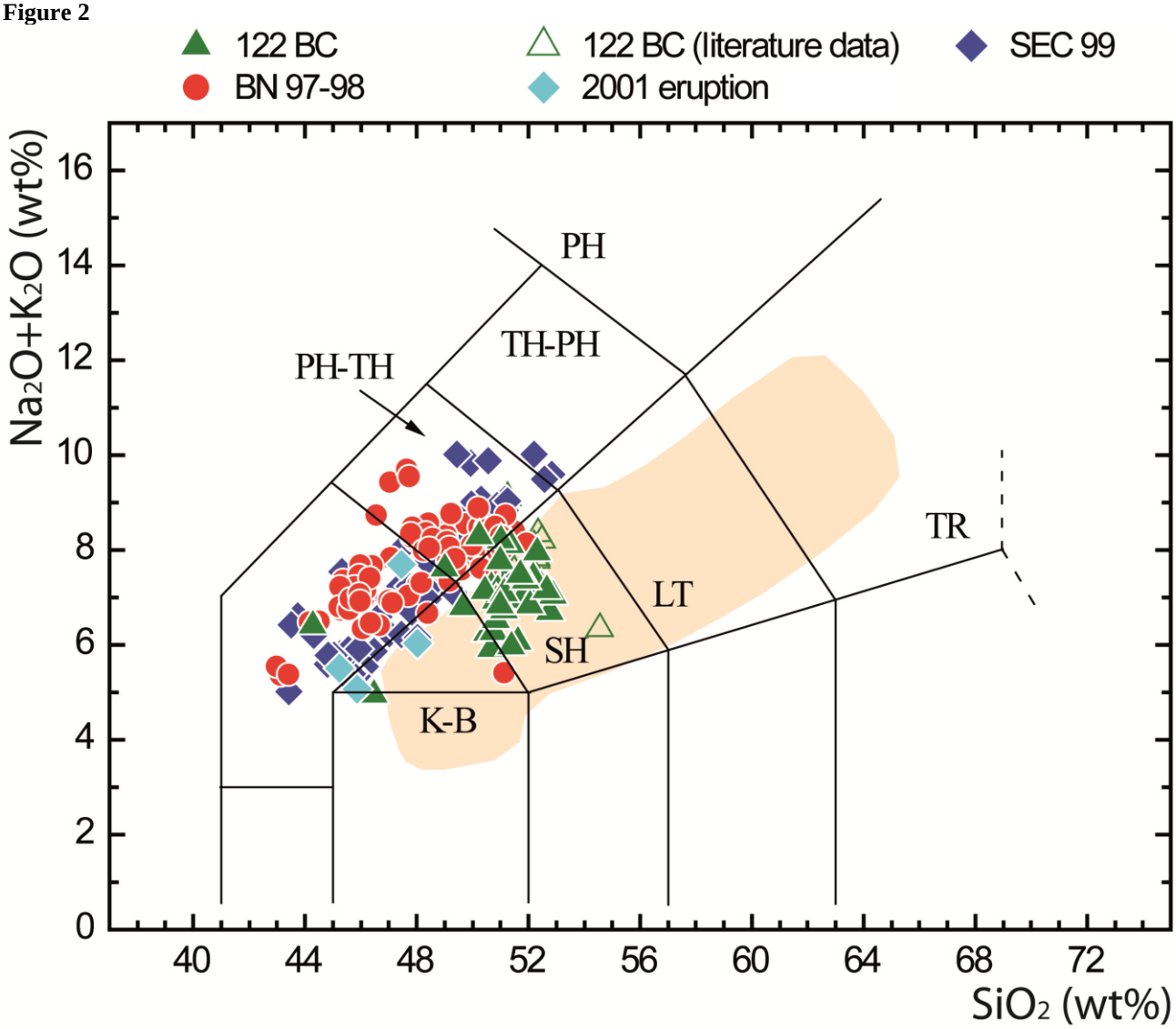

ACCEP

ACCEPTED MANUSCRIPT

Figure 3

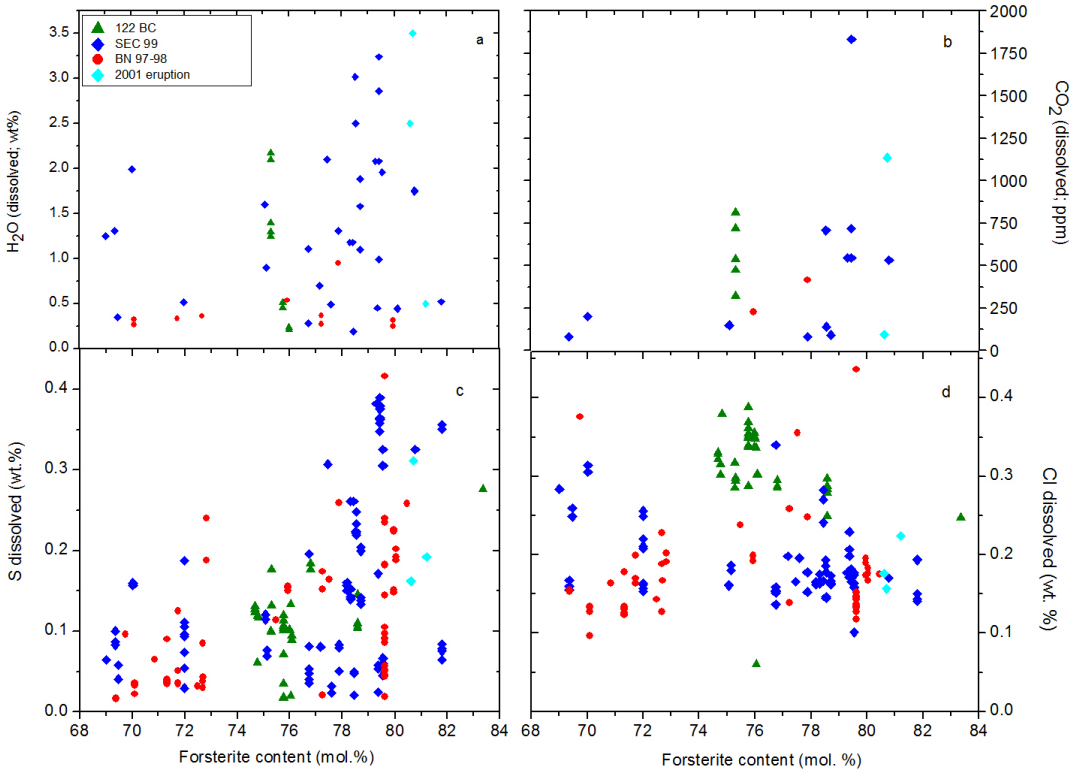

ACCEPTED

ACCEPTED MANUSCRIPT

Figure 4

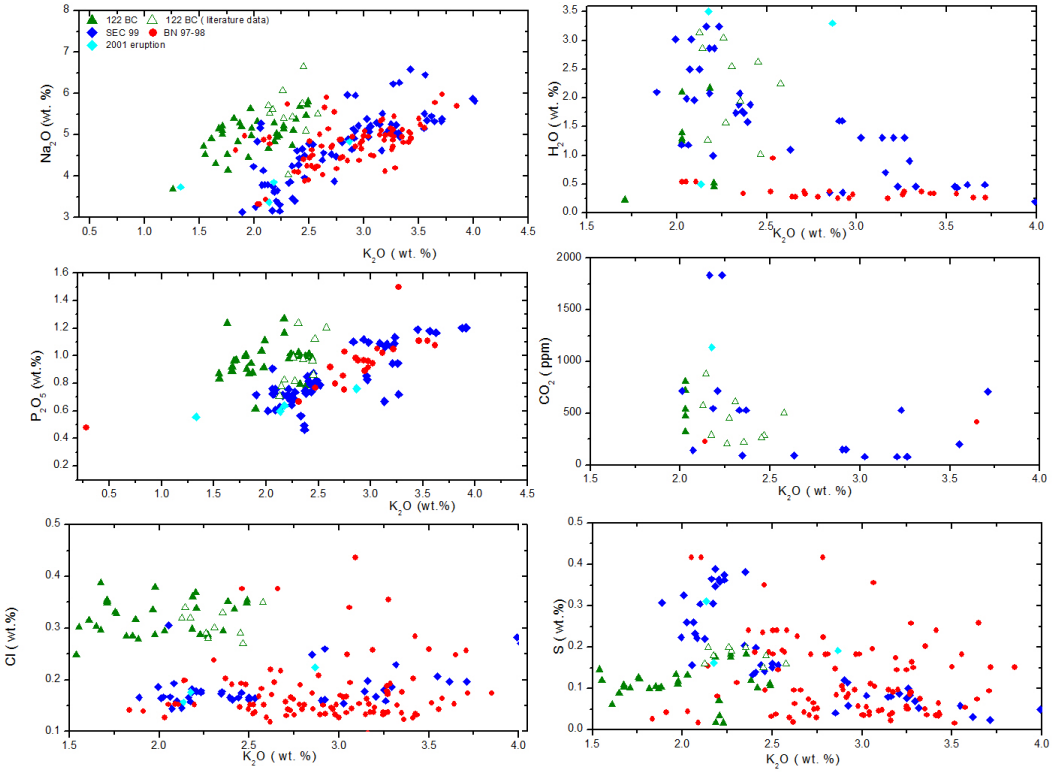

ACCEPTED

ACCEPTED MANUSCRIPT

Figure 5

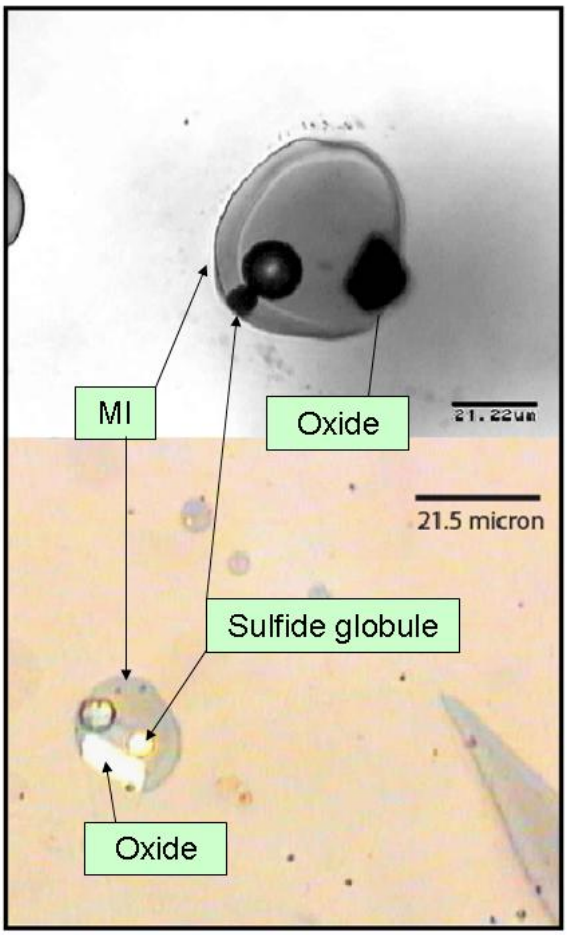

ACCEPTED

ACCEPTED MANUSCRIPT

Figure 6

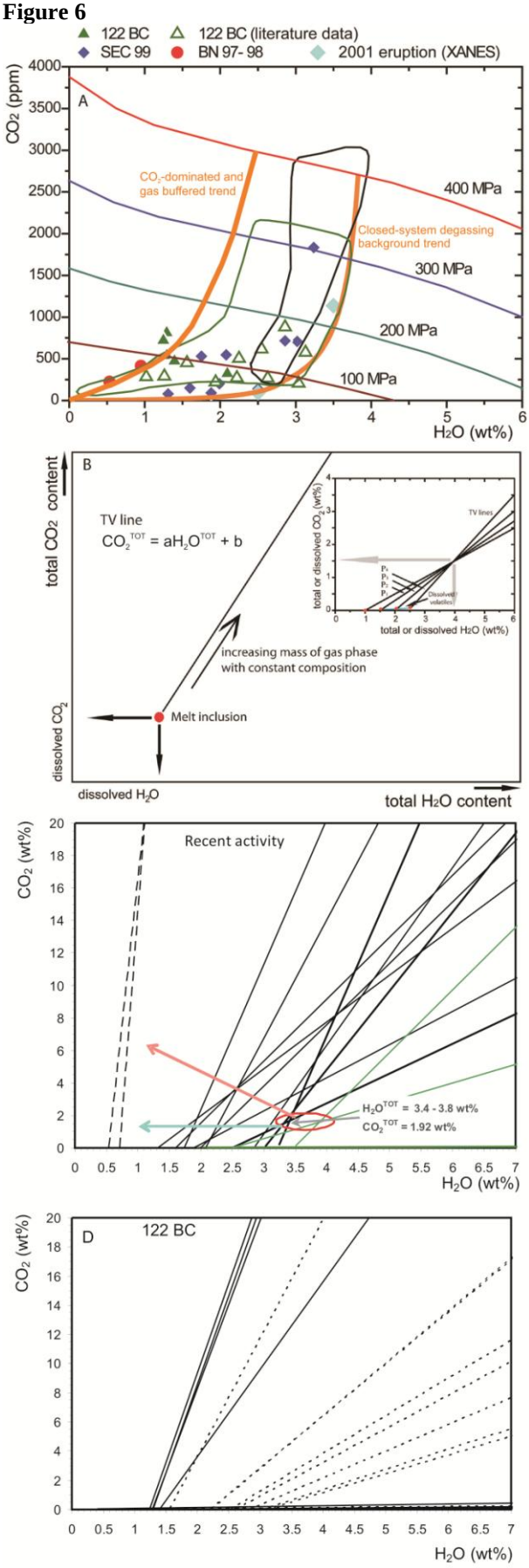

ACCEPTED MANUSCRIPT

Figure 7

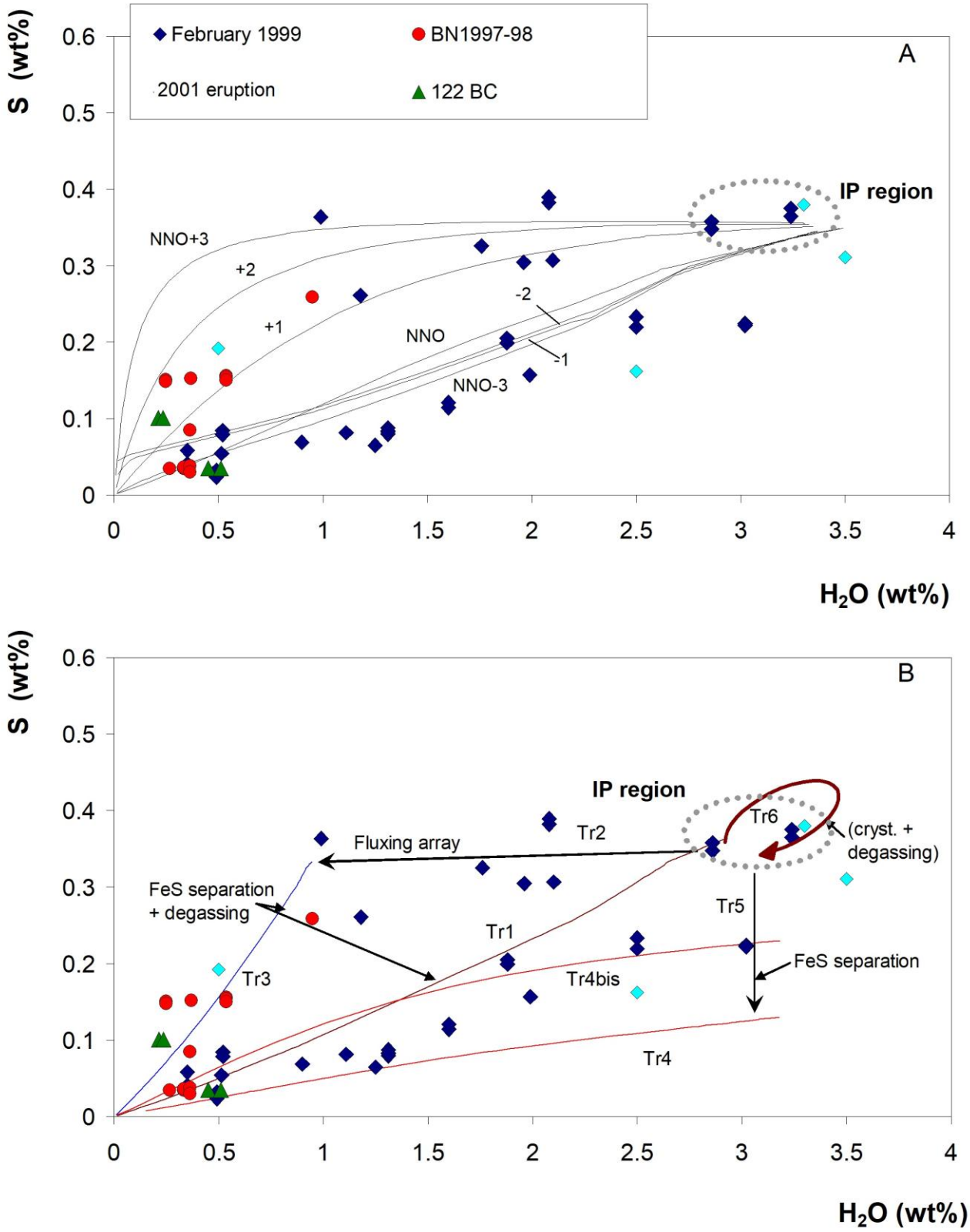

ACCEPTED MANUSCRIPT

Figure 8

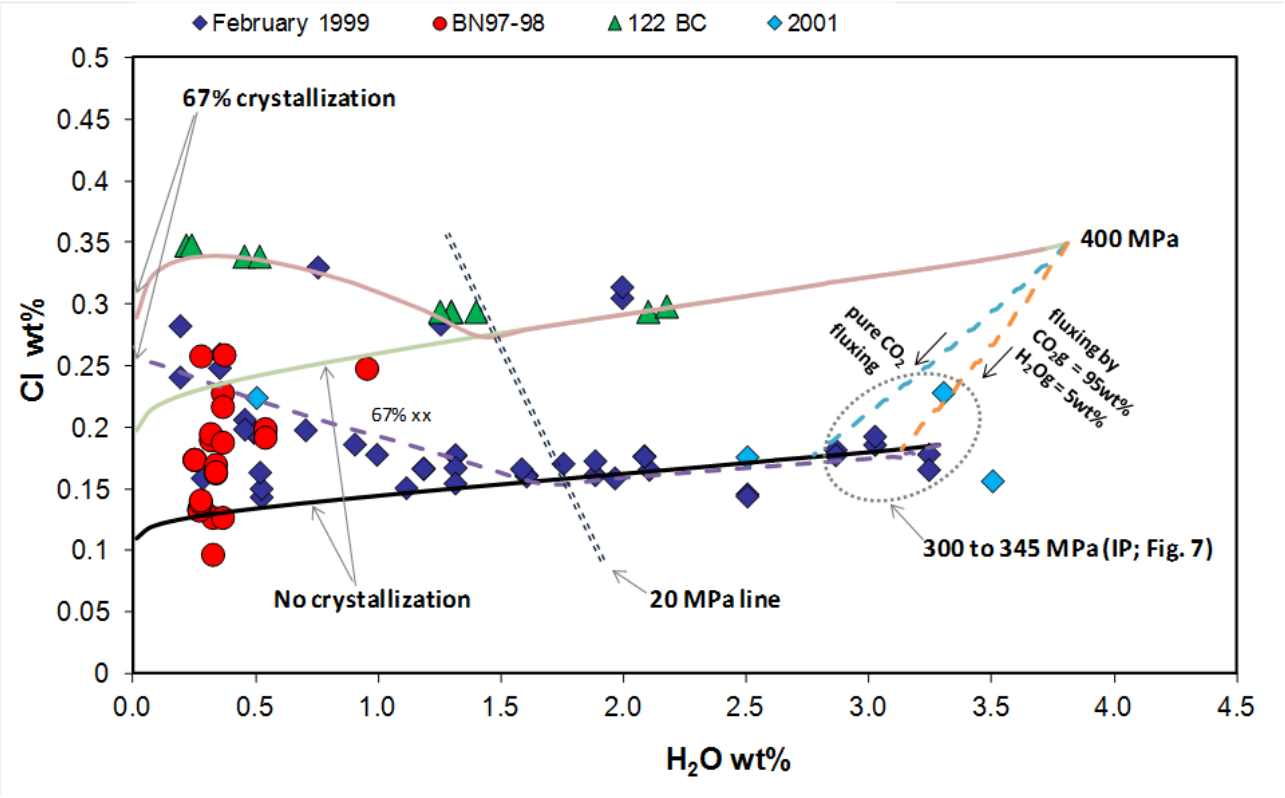

ACCEPTED

ACCEPTED MANUSCRIPT

Figure 9

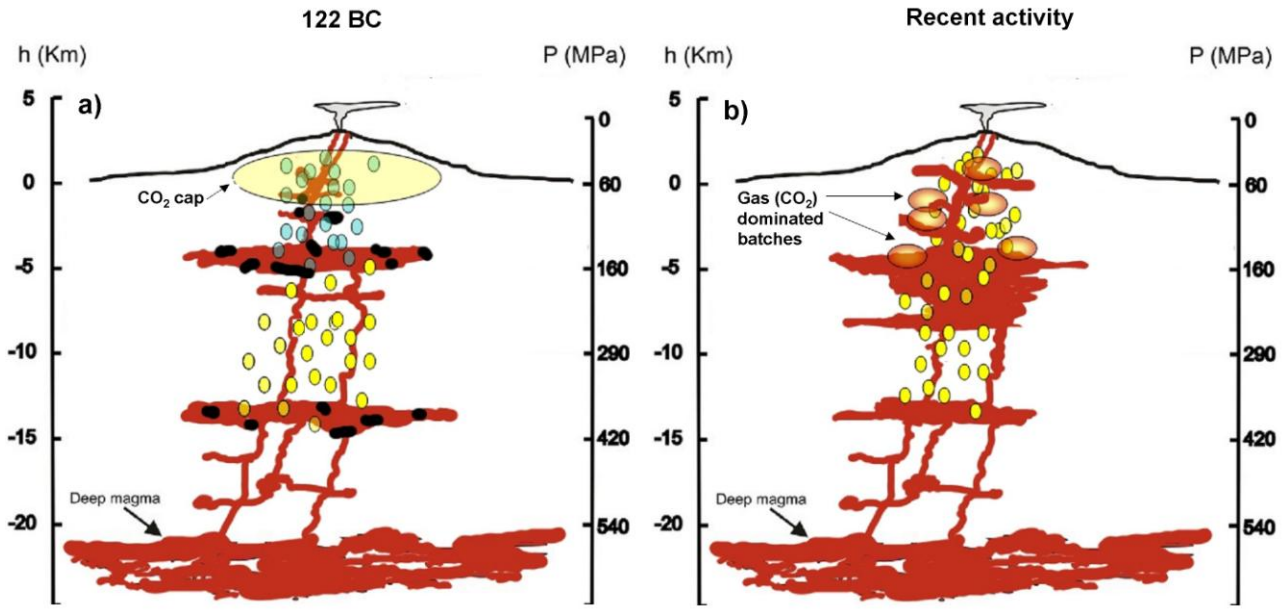

ACCEPTED MANUSCRIPT

ACCEPTED MANUSCRIPT

Figure A1

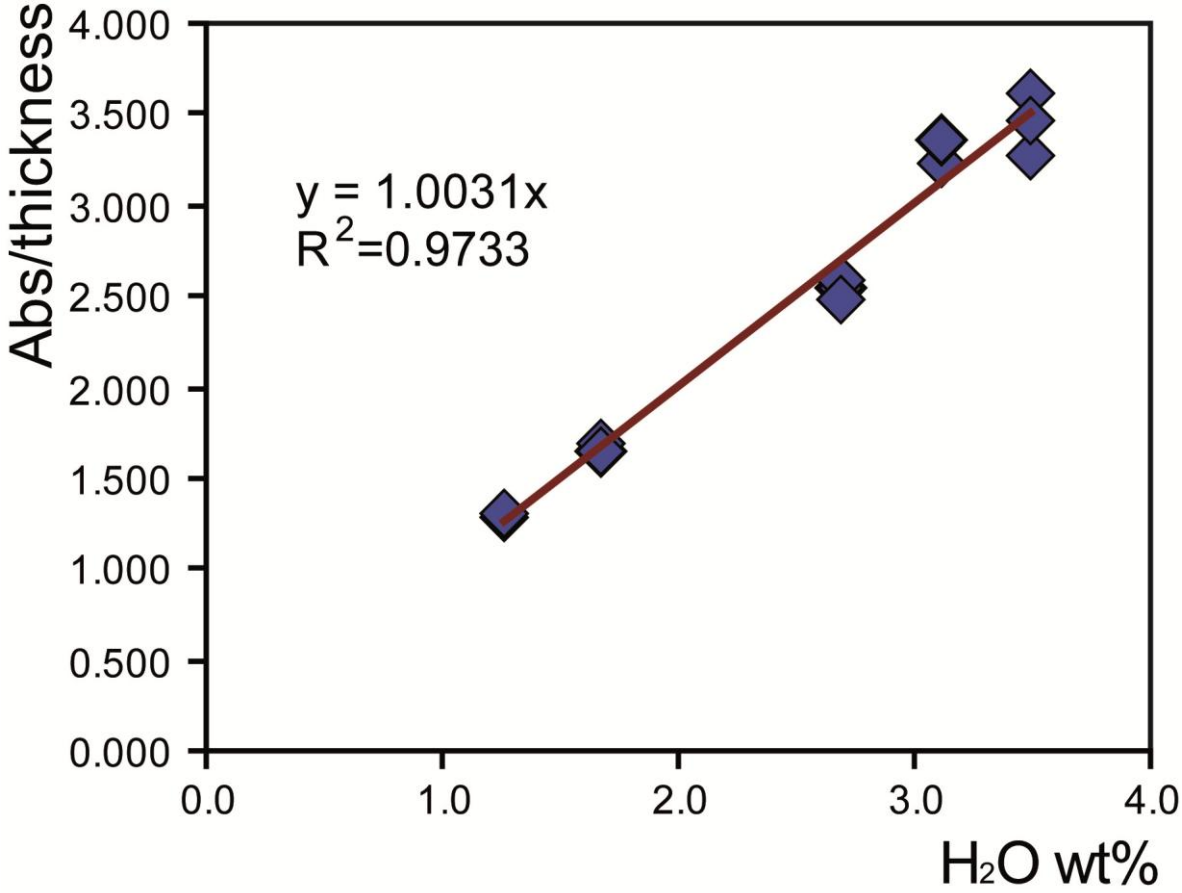

ACCEPTED M

ACCEPTED MANUSCRIPT

Figure A2

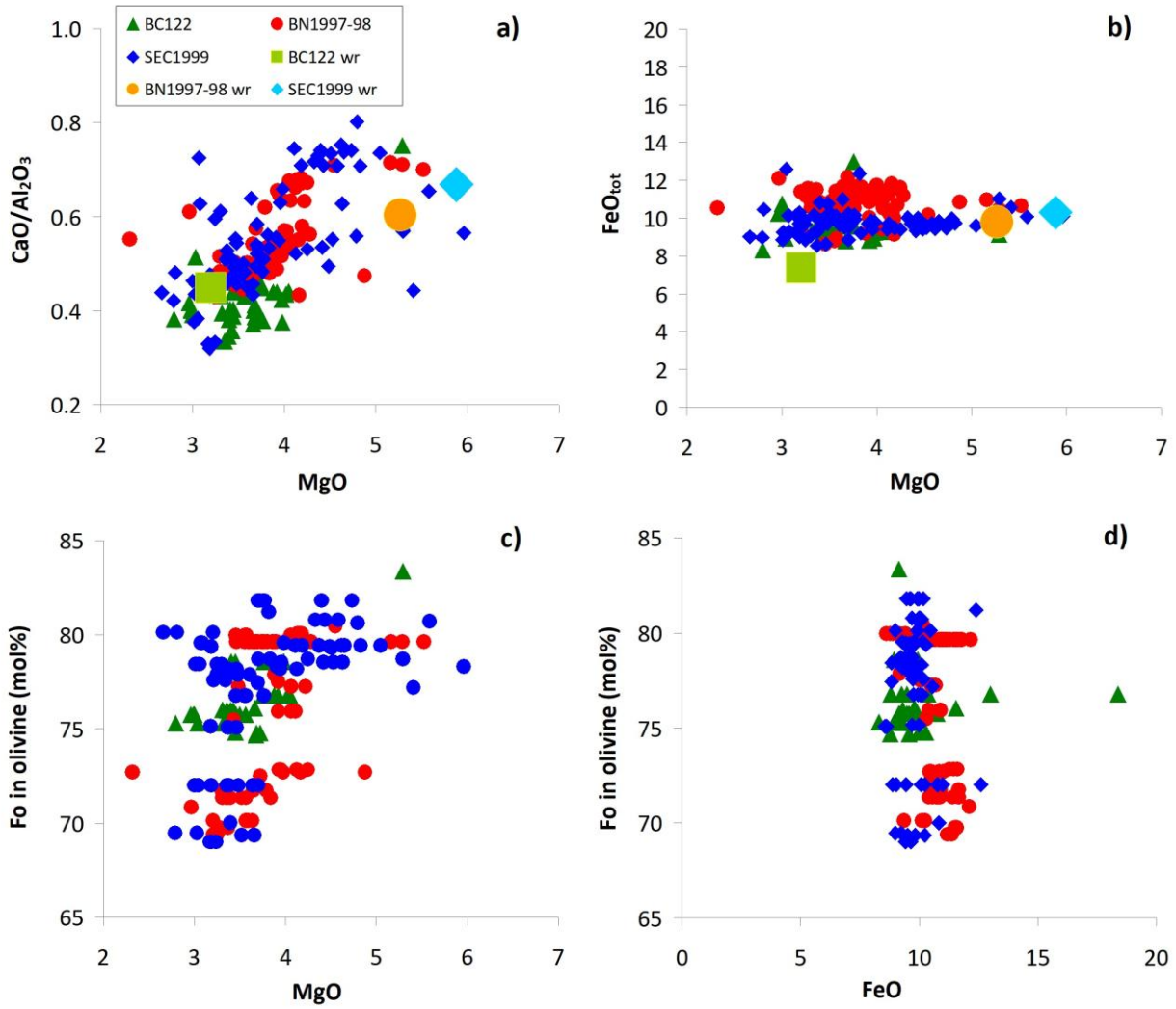

ACCEPTED

ACCEPTED MANUSCRIPT

Figure A3

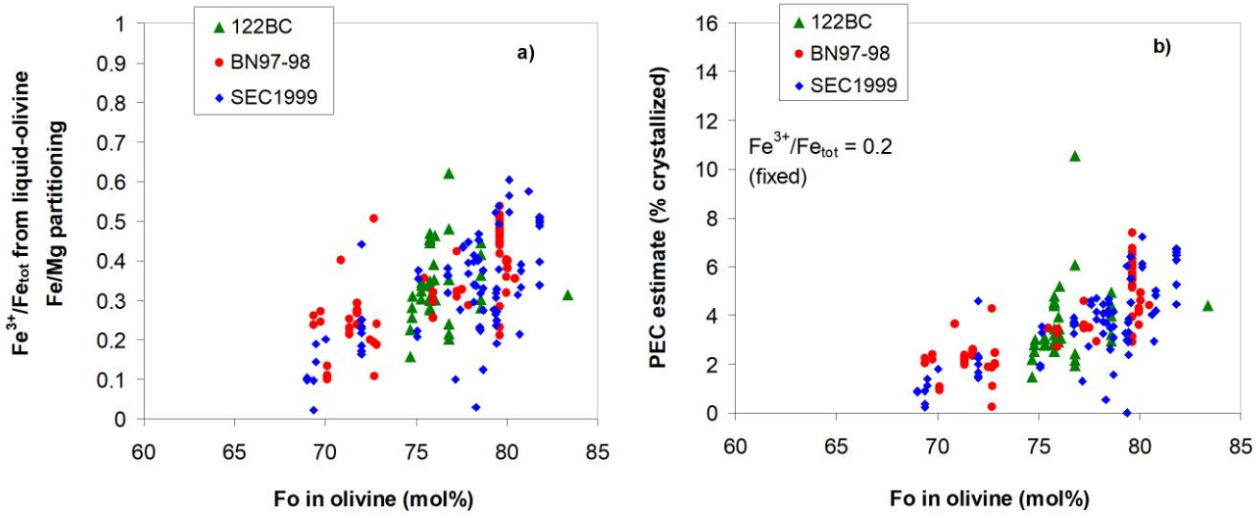

ACCEPTED MANUSC